were processed using Kaluza software (Beckman Coulter) and analyzed with FlowJo (version 7.6.5; TreeStar, Ashland, OR). The total numbers of cells were estimated from a FACS-based cell count of single cell suspensions. Flowcount beads (Beckman-Coulter, Galway, Ireland) were added to the cell samples and cell counts were calculated by the following equation: viable cells × total beads/counted beads.

Cell sorting was performed using a BD FACS Aria III (BD Bioscience). Single cell suspensions were centrifuged over the hypo-osmotic 1.10g/ml density solution OptiPrep (AXIS-SHIELD Poc AS, Oslo, Norway) and recovered from the interphase. Dead cells were excluded in flow cytometry on the basis of forward and side scatter profiles and Fixable Viability Dye eFluor450 (eBioscience). For the cytochemical and reverse transcription–polymerase chain reaction (RT-

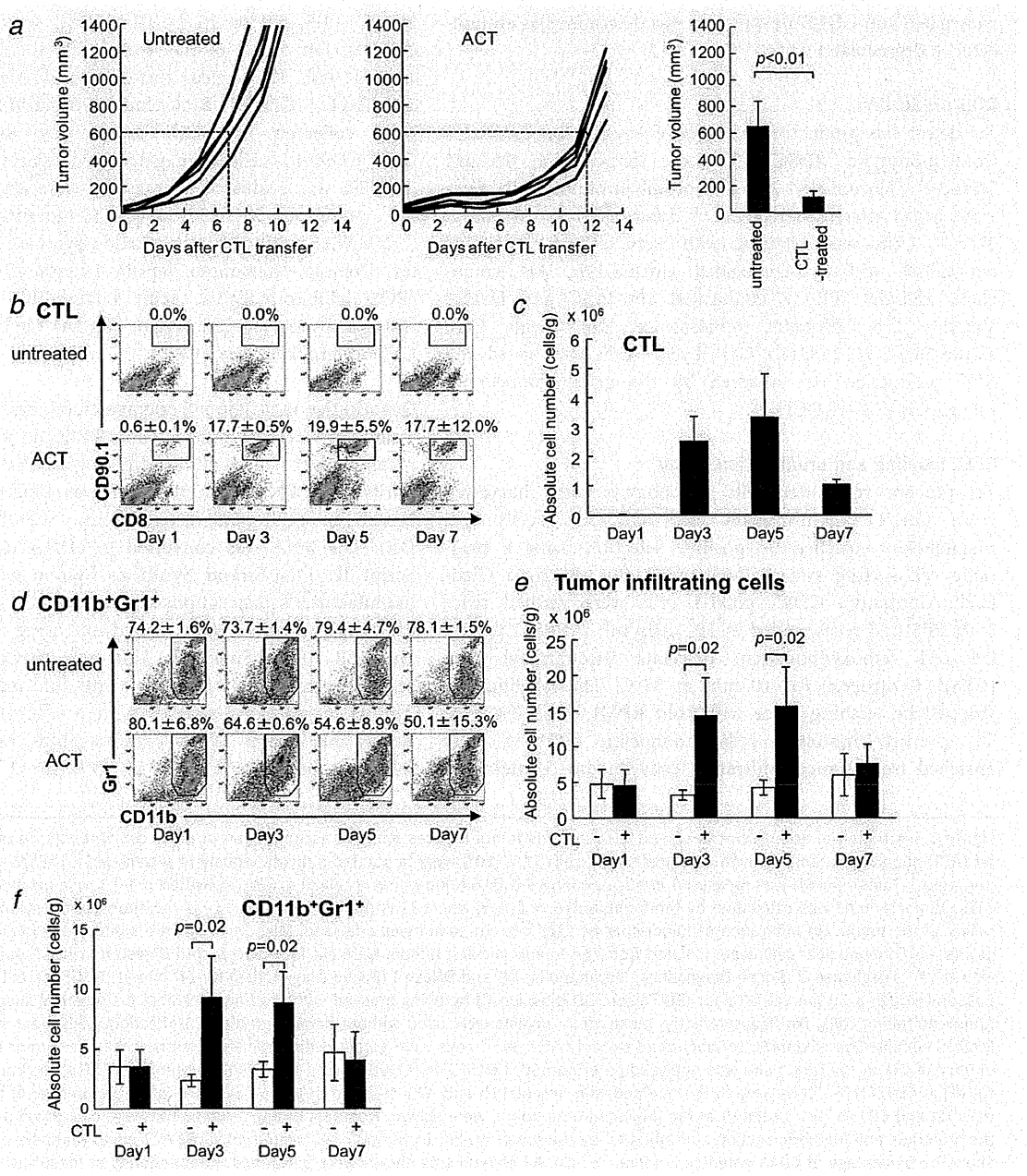

Figure 1.

PCR) analyses, $CD45^-$ tumor and stromal cells, $CD45^+CD11b^+Gr1^{high}Ly6C^{int}$ granulocytic MDSC, $CD45^+CD11b^+Gr\text{-}1^{int/dull}Ly6C^+$ monocytic MDSC, and $CD11b^+Gr\text{-}1^{int/low}Ly6C^-$ macrophage were sorted.

The CD107a externalization assay

To evaluate the cytotoxic function of CTLs, cells (5×10^5) were stimulated for 4 hr with 1 μg/ml mgp100 peptide and 0.5 μl of APC-conjugated anti-CD107a antibody (Biolegend) or isotype control (Rat IgG2a, κ, Biolegend).[15] Cells were stained with Pacific Blue-conjugated anti-CD45, APC-Cy7-conjugated CD8, FITC-conjugated CD90.1. $CD45^+CD8^+CD90.1^+$ cells were gated and CD107a expression was determined as an indicator of degranulation.

ROS production

To detect the production of reactive oxygen species (ROS) from monocytic MDSC, cells were stained with 0.6 μM 5-(and-6)-chloromethyl-2',7'-dichlorodihydrofluorescein diacetate, acetyl ester (CM-H_2DCFDA, Invitrogen) for 30 min at 37°C.[16] Cells were stained with PerCP/Cy5.5-conjugated anti-CD45, APC-Cy7-conjugated anti-CD11b, APC-conjugated anti-Gr1, PE-Cy7-conjugated anti-Ly6C and Fixable Viability Dye eFluor450 (eBioscience, San Diego, CA). $eFluor450^-CD45^+CD11b^+Gr1^{int}Ly6C^+$ cells were gated and ROS production was assessed by the green fluorescence intensity of CM-H_2DCFDA.

CFSE labeling and proliferation assay

To prepare responder cells, splenocytes were harvested from pmel-1 TCR-transgenic mice and $CD8^+$ cells were magnetically enriched by positive selection using a magnetic cell sorting system (Miltenyi Biotec, Bergisch Gladbach, Germany). $CD8^+$ pmel-1 cells were washed twice with PBS and resuspended at 10^7 cells/ml in PBS/1% BSA, 0.6 μM carboxyfluorescein diacetate succinimidyl ester (CFSE, Invitrogen) for 10 min at 37°C. The labeling was stopped by washing twice with cold RPMI with 10% FCS. To prepare inhibitor cells, monocytic MDSCs were enriched from tumor infiltrating cells on day 3 after CTL transfer. Cells were centrifuged over the hypo-osmotic 1.077g/ml density solution OptiPrep (AXIS-SHIELD Poc AS) and cells recovered from the interphase. This procedure eliminates dead cells and granulocytes, including granulocytic MDSC. $CD11b^+$ cells were then isolated using EasySep Mouse CD11b Positive Selection Kits (STEMCELL Technologies, Vancouver, BC) according to the manufacturer's instructions. The purity of monocytic MDSC was routinely >90%. CFSE-labeled pmel-1 cells (5×10^5) were then stimulated for 72 hr in 96-well flat-bottom plates (Greiner Japan, Tokyo, Japan) with hgp100 peptide (1 μg/ml). To assess the immunosuppressive activity of MDSCs, 1.5, 5.0 or 15×10^5 MDSC were added to the cultures. On day 3 of the assay, cells were harvested and stained with PE-labeled anti-CD8 and Alexa 647-labeled anti-Thy1.1 (CD90.1, Biolegend). A total of 100,000 events were collected for each sample by flow cytometry; $CD8^+CD90.1^+$ cells were gated and fluorescence intensity of CFSE was evaluated. The assays were also performed in the presence of 0.5 mM NG-monomethyl-L-arginine (L-NMMA) (inducible nitric oxide synthase (iNOS) inhibitor, Dojindo, Kumamoto, Japan), 10 mM N-acetyl-l-cysteine (ROS inhibitor, Sigma, Saint Louis, MO) and 0.5 mM Nω-hydroxy-nor-l-arginine (Nor-NOHA) (arginase I inhibitor, Calbiochem, San Diego, CA).

Quantitative real-time polymerase chain reaction

Total RNA was extracted using TRIZOL according to the manufacturer's instructions (Invitrogen, Carlsbad, CA). The purity and RNA concentration was determined using a NanoDrop spectrophotometer (Thermo Scientific, Wilmington, DE). The RNA was converted to cDNA using the SuperScript III First-Strand Synthesis System according to the manufacturer's instructions (Invitrogen, Carlsbad, CA), and qRT-PCR reactions were carried out using EXPRESS SYBR GreenER qPCR SuperMix Universal (Invitrogen). Primer sequences are given in Supporting Information Table S1. The PCR reactions were run in a Thermal Cycler Dice Real Time System TP800 (Takara, Shiga, Japan) using the following program: 1 cycle of 95°C for 2 min, 40 cycles

Figure 1. Infiltration of adoptively-transferred CTLs into the tumor induces massive accumulation of other cell types. (*a*) Adoptive CTL transfer (ACT) suppresses tumor growth. B16 melanoma cells (1×10^6) were implanted subcutaneously in 6-week-old C57BL/6 mice (five mice per group). Tumor growth was measured in mice bearing 9-d B16 tumors that received *in vitro* activated pmel-1 splenocytes (1×10^7) as CTLs. Tumor volume was calculated by the formula $\pi/6 \times L_1L_2H$, where L_1 is the long diameter, L_2 is the short diameter, and H is the height of the tumor. (*b*) Infiltration of tumor-specific CTLs into the tumor was analyzed. Mice ($n = 3$) were killed at the indicated time points and mononuclear cells were isolated from the tumor. In brief, tumors were cut into pieces, and digested in HBSS supplemented with 0.1% collagenase D (Roche Diagnostics, Indianapolis, IN) and DNase I (Roche Diagnostics) for 60 min at 37°C. The entire material was passed through a 70 μm cell strainer (BD Falcon, BD Bioscience) by being pressed with a plunger, to obtain single cell suspensions of tumor-infiltrating cells. For flow cytometry, these tumor digests were used without density gradient purification. Cells were stained with Fixable Viability Dye eFluor450 to label dead cells. Then, $CD45^+$ cells were gated to discriminate immune cells form tumor cells. The frequency of CTL at the tumor site was analyzed as $eFluor450^-CD45^+CD8^+CD90.1^+$ and the absolute number of CTLs was calculated (*c*). (*d*) $eFluor450^-CD45^+$ cells were further stained with anti-CD11b and -Gr1 mAbs to detect MDSCs. The absolute number of tumor infiltrating cells (*e*) and $CD11b^+Gr1^+$ cells (*f*) at the indicated time points were shown. Numbers of each population were calculated as described in the Materials and Methods section and adjusted by the tumor weight (cells/g). □ untreated mice, ■ ACT mice. Numbers on the images show the percentage of CD45 gated cells (mean ± SD). All experiments shown were performed independently at least three times with similar results.

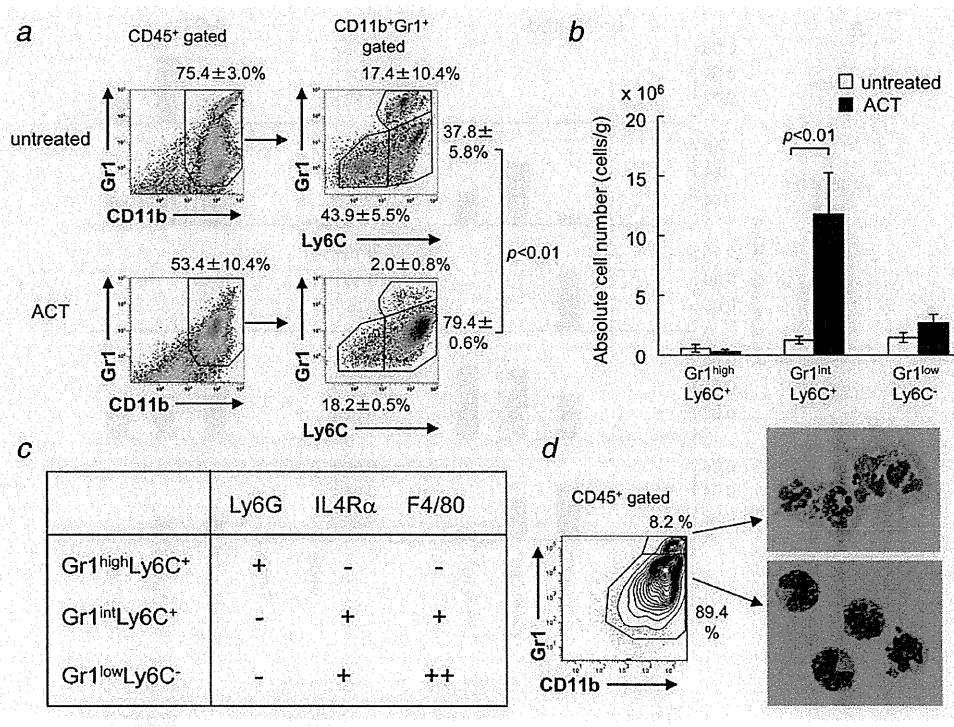

Figure 2. The characteristic phenotype of CTL-induced MDSCs. Tumor-bearing mice (n = 4) were treated as described in Figure 1. Tumor–infiltrating cells were harvested 3 days after ACT and analyzed by flow cytometry. (*a*) eFluor450$^-$CD45$^+$CD11b$^+$Gr1$^+$ cells were further defined by the expression of Ly6C. Numbers on the top of the images show the percentage of gated cells (mean ± SD). (*b*) Numbers of Gr1^{high}Ly6C$^+$, Gr1^{int}Ly6C$^+$ and Gr1^{low}Ly6C$^-$ cells were compared w/o ACT. □ untreated mice, ■ ACT mice. (*c*) Surface phenotypes of MDSCs were further defined by the expression of Ly6G, IL-4Rα and F4/80. (*d*) CD11b$^+$Gr1^{high} and CD11b$^+$Gr1^{int}cells were sorted from day 3 infiltrates from ACT mice (n = 5), stained with Diff quick as described in Materials and Methods; their morphology was assessed using an OLYMPUS BX41 microscope. All experiments shown were performed independently at least three times with similar results. [Color figure can be viewed in the online issue, which is available at wileyonlinelibrary.com.]

95°C for 15 sec, 60°C for 30 sec. Results are expressed as ratios. The quantity of target mRNA was normalized to the level of GAPDH in each sample. PCR was performed in duplicate for each experiment and the PCR products were also monitored by electrophoresis on 1.8% agarose gels and visualized with ethidium bromide.

Cytology

Smears were prepared from each sorted cell population, air dried, and stained with Diff quick (Sysmex, Kobe, Japan) according to the manufacturer's instructions. Cell morphology was evaluated using bright field microscopy (OLYMPUS BX41 with Canon EOS Kiss X4 digital camera, OLYMPUS, Tokyo, Japan, magnification 1,000×).

Histologic analysis

Fresh frozen sections were stained as described previously.[17] In brief, cryosections were fixed in ice-cold acetone and preincubated in Block Ace (Dainippon Pharmaceutical, Tokyo, Japan). Subsequently, samples were incubated with primary antibodies or appropriate control antibodies, followed by appropriate Alexa Fluor-labeled secondary reagents (Invitrogen Japan K.K., Tokyo, Japan). The samples were then analyzed using BZ-9000 fluorescence microscope with BZ-II image processing software (KEYENCE, Osaka, Japan). Purified anti-mouse F4/80, FITC-conjugated Ly6C, APC-conjugated CD90.1, anti-APC-biotin were purchased from Biolegend. Goat anti-Rat IgG-Alexa 546, Rabbit anti-FITC Alexa 488, Donkey anti-Rabbit 488, Streptavidin-Alexa 647 were purchased from Invitrogen. Tissues were also fixed in 10% neutral formalin (Muto Pure Chemicals, Tokyo, Japan), embedded in paraffin, sectioned (3 mm), and stained with hematoxylin and eosin.

Statistical analysis

Statistical analyses were performed with JMP software, version 9.0.0. (SAS Institute Inc., Cary, NC). Results are shown as mean ± SD. Comparison of results was carried out using the two-tailed unpaired t-test.

Results

Adoptively-transferred CTLs migrate to the tumor and induce accumulation of myeloid cells

To investigate the mechanisms responsible for effective immunotherapy, we utilized a murine model with B16

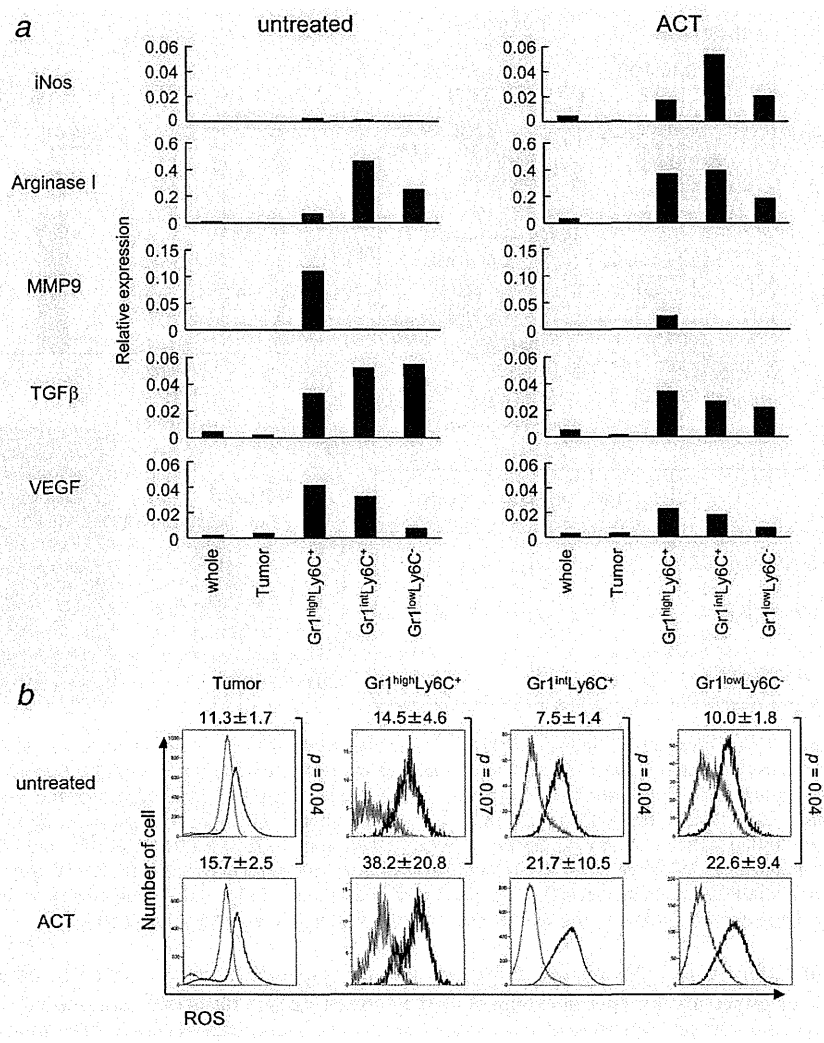

Figure 3. Immunosuppressive effector molecules of MDSCs. (*a*) Tumor-bearing mice (n = 3) were treated as described in Figure 1. Tumor-infiltrating cells were harvested 3 days after CTL transfer, pooled and stained with eFluor450, ant-CD45-FITC, anti-CD11b-APC/Cy7, anti-Gr1-APC and anti-Ly6C-PE/Cy7. $CD45^-$ tumor cells, $Gr1^{high}Ly6C^+$ granulocytic MDSC, $Gr1^{int}Ly6C^+$ monocytic MDSC and $Gr1^{low}Ly6C^-$ cells were sorted and mRNA was isolated. The messages for iNOS, arginase I, MMP9, TGFβ and VEGF were analyzed by quantitative RT-PCR. (*b*) Tumor-infiltrating cells were stained with anti-CD45-PerCP/Cy5.5, anti-CD11b-APC/Cy7, anti-Gr1-APC, anti-Ly6C-PE/Cy7 and CM-H_2DCFDA; ROS expression was compared with the green fluorescence intensity. Numbers on the top of the images show the fluorescent intensity (mean ± SD). All experiments shown were performed independently at least three times with similar results.

melanoma cells and pmel-1-TCR transgenic T cells. As shown in Figure 1*a*, tumors grew progressively in untreated mice. In contrast, tumor growth was suppressed in mice receiving CTLs by adoptive transfer. On day 7, the tumor volume in untreated and CTL-treated (designated as ACT) animals was 654.9 ± 185.4 mm^3 and 122.6 ± 40.5 mm^3, respectively ($p < 0.01$). While tumors exceeded 600 mm^3 by day 6.8 ± 0.9 in untreated mice, this took 11.7 ± 0.5 days in ACT mice ($p < 0.01$). These results indicate that adoptively-transferred CTLs cause a significant delay in tumor growth. However, anti-tumor activity was transient and tumors started to grow again around day 8.

To investigate the underlying mechanisms that limit the duration of anti-tumor activity of these infused CTLs, dynamic changes in the cells present within the tumor were analyzed. Tumors were isolated from untreated or ACT mice at the indicated time points after CTL transfer and were examined by histology with standard hematoxylin-eosin staining (Supporting Information Fig. S1). Only scattered inflammatory infiltrates were observed in the tumor from untreated mice and ACT mice on day 1. Massive infiltration of mononuclear cells and destruction of tumor cells were observed on day 3 and 5 after CTL transfer. The inflammatory response slightly subsided on day 7. To further investigate the tumor infiltrating cells, mice

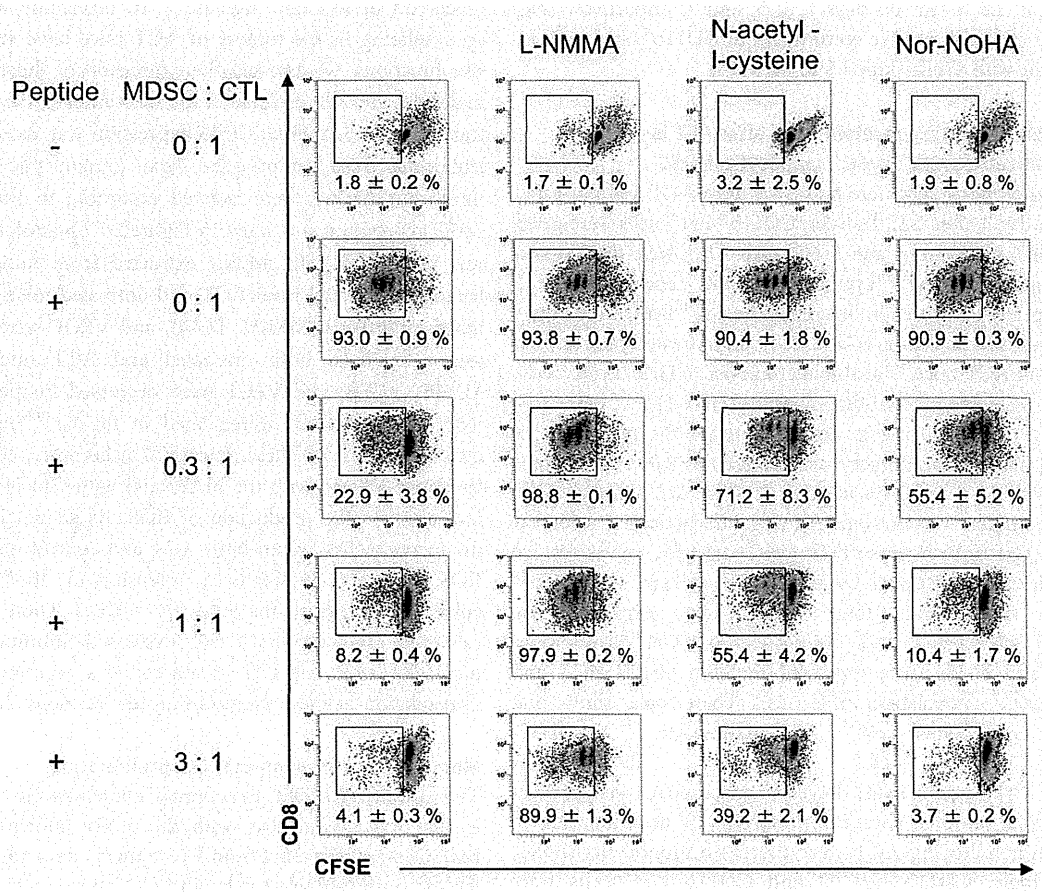

Figure 4. MDSCs inhibit the proliferation of antigen-specific CTLs. Tumor-bearing mice (n = 10) were treated as described in Figure 1. Tumor-infiltrating cells were harvested from B16 tumor 3 days after CTL transfer and MDSCs were positively selected by anti-CD11b magnetic beads. CFSE-labeled pmel-1 cells were stimulated with hgp100 peptide in the presence or absence of MDSCs at the indicated ratio. The proliferation of pmel-1 cells was evaluated by flow cytometry. The proliferation of pmel-1 cells was further studied in the presence of L-NMMA (iNOS inhibitor), *N*-acetyl-L-cysteine (ROS inhibitor) and Nor-NOHA (arginase I inhibitor). Numbers on the images show the percentage of gated cells (mean ± SD). All experiments shown were performed independently at least three times with similar results.

were sacrificed at different time points after infusing CTLs and mononuclear cells were isolated from their tumors. The cells were stained with eFluor450 to label dead cells and the percentages and numbers of eFluor450$^-$CD45$^+$ cells were analyzed by flow cytometry (Fig. 1). Adoptively-transferred CTLs preferentially infiltrated into the tumor. In ACT mice, CD8$^+$CD90.1$^+$ CTLs were detected in the tumor as early as day 1 after CTL transfer, peaked on day 3 to 5 and gradually decreased by day 7 (Figs. 1*b* and 1*c*). The presence of CTLs in the tumor paralleled the inhibition of tumor growth observed in these ACT mice.

In untreated mice on day 1, the percentages of CD8$^+$, CD4$^+$ and NK1.1$^+$ cells in the tumor were approximately 3.8 ± 2.1%, 5.3 ± 1.3% and 3.2 ± 1.4%, respectively (Supporting Information Fig. S2). The percentage of CD11b$^+$Gr1$^+$ cells was 74.2 ± 1.6% (Fig. 1*d*). Thus, the majority of tumor-infiltrating cells were not lymphocytes but consisted of CD11b$^+$Gr1$^+$ myeloid cells. In ACT mice, the tumor-infiltrating CTLs were accompanied by massive accumulation of other cells (Fig. 1*e*). While about 5.0 × 10^6 cells per gram tumor weight were harvested from B16 tumors in untreated mice, we obtained 1.4 ± 0.5 × 10^7 and 1.6 ± 0.5 × 10^7 from ACT mice on day 3 and 5, respectively (Fig. 1*e*). CTL transfer did not affect the frequency of recipient-derived CD8$^+$ (eFluor450$^-$CD45$^+$CD8$^+$CD90.1$^-$) and CD4$^+$ T cells (Supporting Information Figs. S2A and B). However, the absolute numbers of these cells were increased. The frequency and number of NK cells (eFluor450$^-$CD45$^+$NK1.1$^+$) in the tumor slowly increased after CTL transfer (Supporting Information Fig. S2C). Of note, massive accumulation of CD11b$^+$Gr1$^+$ cells was observed in the tumor (Figs. 1*d* and 1*f*). This was not reflected in an increased percentage of CD11b$^+$Gr1$^+$ cells in the tumor relative to the untreated animals, but the absolute number of these cells in ACT mice was much greater (p = 0.02) (Fig. 1*f*). The numbers of CD11b$^+$Gr1$^+$ cells in ACT mice were 3.6 ± 1.4 × 10^6, 9.3 ± 3.4 × 10^6, 8.9 ± 2.2 × 10^6,

and 4.1 ± 2.3 × 10^6 on days 1, 3, 5, and 7, respectively (Fig. 1*f*). ACT induced massive recruitment of $CD11b^+Gr1^+$ cells in the tumor with similar kinetics to the CTLs.

Increased infiltrating myeloid cells after ACT is characterized as $Gr1^{int}Ly6C^+$ monocytic MDSC

Tumor-infiltrating cells were harvested from ACT and untreated mice on day 3 after CTL transfer; $CD11b^+Gr1^+$ cells were gated and further analyzed by anti-Ly6C mAb. They were divided into three populations, $Gr1^{high}Ly6C^+$, $Gr1^{int}Ly6C^+$ and $Gr1^{low}Ly6C^-$ cells (Fig. 2*a*). As shown in Figure 2*a*, the $Gr1^{int}Ly6C^+$ cell population was increased from 37.8 ± 5.8% in untreated mice to 79.4 ± 0.6% in ACT mice. The absolute number of $Gr1^{int}Ly6C^+$ cells in ACT mice was 9.2-fold that of control mice (1.2 ± 0.3 × 10^7 *vs.* 1.3 ± 0.3 × 10^6) (Fig. 2*b*). In contrast, the percentage of $Gr1^{high}Ly6C^+$ in ACT mice was decreased to 2.0 ± 0.8% compared with 17.4 ± 10.4% in controls (Fig. 2*a*), although their absolute number was not different (Fig. 2*b*). Because it is known that the Gr1 mAb binds to both Ly6G and Ly6C molecules, we further defined these cells by anti-Ly6G and Ly6C mAbs separately. We found that Ly6G was expressed by $CD11b^+Gr1^{high}Ly6C^+$ cells, but not $CD11b^+$ $Gr1^{int}Ly6C^+$ cells. IL4Rα and F4/80 were expressed by both $Gr1^{int}Ly6C^+$ and $Gr1^{low}Ly6C^-$ populations (Fig. 2*c*). These data show that $CD11b^+Gr1^{high}Ly6G^+Ly6C^+$ granulocytic MDSC, $CD11b^+Gr1^{int}Ly6G^-Ly6C^+$ monocytic MDSC and $CD11b^+Gr1^{low}Ly6G^-Ly6C^-F4/80^{++}$ macrophage were present in the B16 tumors. The cells preferentially accumulating in the tumor following ACT were therefore monocytic MDSC. Accordingly, $CD11b^+Gr1^{high}$ and $CD11b^+Gr1^{int}$cells were sorted from day 3 infiltrating cells from ACT mice and their morphology examined by light microscopy (Fig. 2*d*). Multilobed or polymorph nuclei were observed in $CD11b^+Gr1^{high}$ cells and eccentrically-placed kidney bean-shaped nuclei in $CD11b^+Gr1^{int}$ cells. Consistent with these single cell analysis, infiltration of adoptively-transferred CTLs and recruitment of monocytic MDSCs were observed in the tumor after ACT by immunohistochemistry (Supporting Information Fig. S3). While only a few $CD90.1^+$ CTLs (blue) were detected in the tumor on day1, diffuse infiltration of CTLs were observed in the tumor on day 3 to 7. Infiltration of CTLs were accompanied by 3-5 times more in number of the recruitment of $Ly6C^+$ monocytic MDSCs (green). The distribution of $CD90.1^+$ CTLs, $Ly6C^+$ monocytic MDSCs, and $F4/80^+$ macrophages were compared between the center and the peripery of the tumor on day 3 (Supporting Information Fig.S4). CTLs and macropahges distributed throughout the tumor tissue in a disseminated manner as scattered solitary cells. Aggregates and condensations of monocytic MDSC co-localized with CTLs. These results suggested that tumor infiltrating CTLs recruited monocytic MDSC.

Adoptively-transferred CTLs activate monocytic MDSC

It has been reported that granulocytic MDSC use ROS to mediate suppression,[18] whereas monocytic MDSC use up-regulation of NO and arginase.[19] To determine whether cells accumulating in the tumors of ACT mice have such suppressive functions, we assessed the expression of these suppressive molecules by cells isolated from the tumor 3 days after CTL transfer (Fig. 3*a*). First, CD45 expression was used to separate leukocytes from tumor cells. Next, granulocytic MDSC and monocytic MDSC were isolated according to their Gr1 and Ly6C expression as defined in Figure 2*a*. Quantitative RT-PCR was performed with mRNA extracted from tumor cells and leukocytes isolated from ACT and untreated mice. mRNAs for iNOS, arginase I, MMP9, TGFβ, and VEGF were detected in leukocytes from both untreated and ACT mice. Although MMP9, TGFβ, and VEGF were decreased in the ACT mice, iNOS was markedly upregulated in the $Gr1^{int}Ly6C^+$ monocytic MDSCs from these animals. Furthermore, cells were isolated and stained with the mAbs and with CM-H_2DCFDA, an indicator for the production of ROS. As shown in Figure 3*b*, monocytic MDSC from both ACT and control mice produced ROS, but the fluorescence intensity of the former was enhanced relative to the latter ($p = 0.04$). These results indicate that monocytic MDSC expressed immunosuppressive molecules and that CTL treatment was accompanied by an upregulation of these immunosuppressive molecules in MDSC.

Monocytic MDSC suppress CTL proliferation

The capacity of MDSC to suppress antigen-specific T-cell proliferation was investigated, with the results shown in Figure 4. MDSCs were harvested from B16 tumor 3 days after CTL transfer and positively selected by anti-CD11b magnetic beads. Their purity was 91.6% (data not shown). To prepare responder cells, gp100-specific T cells were isolated from pmel-1 TCR transgenic mice (designated pmel-1 cells) and labeled with CFSE. MDSCs were pulsed with 1 μg/ml hgp100 peptide and co-cultured with CFSE-labeled pmel-1 cells for 3 days. Pmel-1 spleen cells did not proliferate without peptide (Fig. 4, upper left). In the presence of peptide and without MDSCs, 93.0 ± 0.9% of pmel-1 cells experienced cell division within 3 days. When MDSCs were added to the cultures, proliferation was inhibited in a dose-dependent manner. When MDSCs were incubated with pmel-1 cells at a ratio of 0.3:1, 1:1 or 3:1, 22.9 ± 3.8%, 8.2 ± 0.4%, 4.1 ± 0.3% of pmel-1 cells divided, respectively. These results indicate that MDSCs in the tumors of ACT mice inhibited the proliferation of the infused antigen-specific CTLs.

To identify the factors responsible for the immunosuppressive activity of these MDSC, blockade of pmel-1 cell proliferation was tested in the presence of L-NMMA (iNOS inhibitor), *N*-acetyl-L-cysteine (ROS inhibitor) or Nor-NOHA (arginase I inhibitor). By themselves, these reagents had no effect on pmel-1 proliferation at the concentrations used (Fig. 4, upper two lanes). However, in the presence of L-NMMA, inhibition of pmel-1 proliferation by MDSC was completely abrogated. Even when three times more MDSCs were added to the culture, 89.9 ± 1.3% of pmel-1 cells still proliferated.

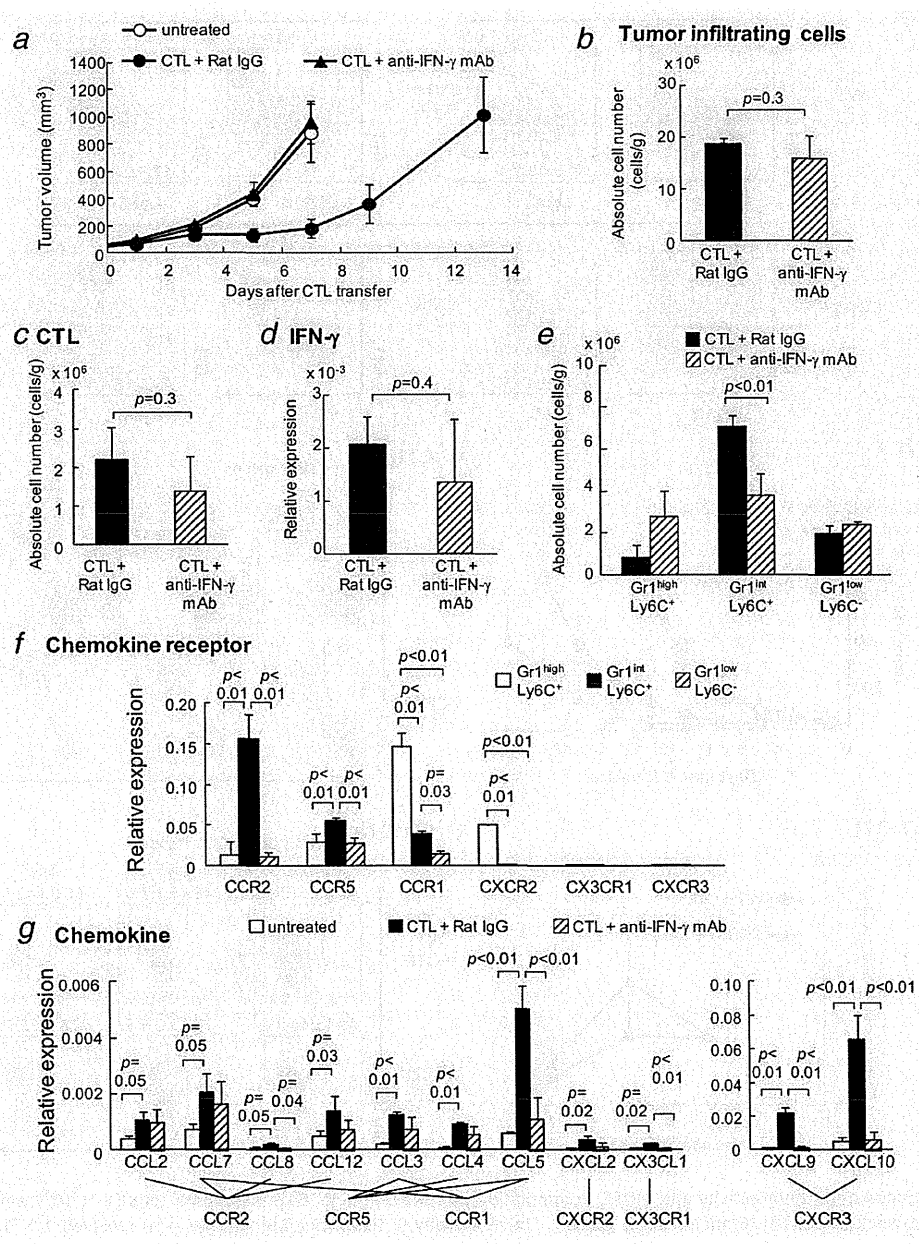

Figure 5. The anti-tumor activity of CTLs and the accumulation of monocytic MDSCs is mediated by IFN-γ. B16 melanoma cells (1×10^6) were implanted subcutaneously in 6-week-old C57BL/6 mice (six or seven mice per group). Tumor growth was measured in mice bearing 9-d B16 tumors that received 1×10^7 CTLs activated *in vitro*. ACT mice were divided into two groups; one received anti-IFN-γ mAb and the other received control Rat IgG_1. (*a*) Tumor volume was compared between untreated and ACT mice w/o anti-IFN-γ mAb treatment. Tumor-infiltrating cells were harvested 3 days after ACT. The number of tumor-infiltrating cells (*b*) and CTLs (*c*) and intratumoral expression of IFN-γ mRNA (*d*) were compared between IFN-γ-treated or control IgG-treated mice after ACT. (*e*) The number of $Gr1^{high}Ly6C^+$ granulocytic MDSC, $Gr1^{int}Ly6C^+$ monocytic MDSC and $Gr1^{low}Ly6C^-$ cells were also compared. ■ CTL + Rat IgG-treated mice, ▨ CTL + anti-IFN-γ mAb-treated mice. (*f*) $Gr1^{high}Ly6C^+$ *granulocytic MDSC*, $Gr1^{int}Ly6C^+$ *monocytic MDSC and* $Gr1^{low}Ly6C^-$ *cells were sorted from ACT mice without anti-IFN-γ* mAb 3 days after CTL transfer and RNA was isolated. The messages for chemokine receptors, CCR2, CCR5, CCR1, CXCR2, CX3CR1 and CXCR3, were compared in these cell populations (□ $Gr1^{high}Ly6C^+$, ■ $Gr1^{int}Ly6C^+$, ▨ $Gr1^{low}Ly6C^-$ cells) by quantitative RT-PCR. (*g*) Tumors were harvested on day 3 after CTL transfer and total RNA was isolated. The mRNA expression of chemokines, CCL2, CCL7, CCL8, CCL12, CCL3, CCL4, CCL5, CXCL2, CX3CL1, CXCL9 and CXCL10, were compared with these animals (□ untreated, ■ CTL + Rat IgG-treated mice, ▨ CTL + anti-IFN-γ mAb-treated mice) by qRT-PCR. All experiments shown were performed independently at least three times with similar results.

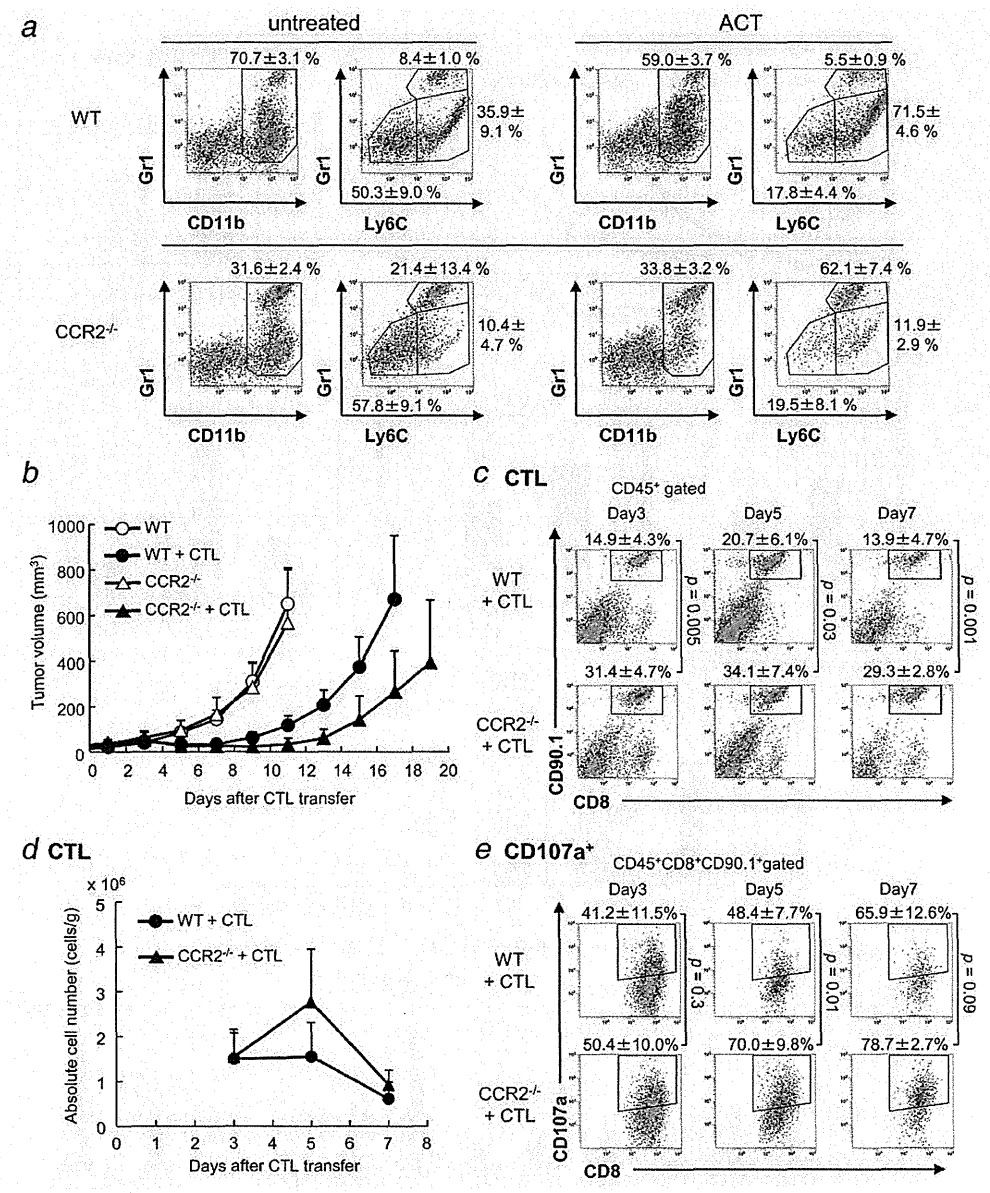

Figure 6. CTL-induced anti-tumor activity and MDSC accumulation in CCR2$^{-/-}$ mice. B16 melanoma cells (1×10^6) were implanted subcutaneously in 6-week-old C57BL/6 mice (WT) or CCR2$^{-/-}$ mice. On day 9, tumor-bearing mice ($n = 4$) received 1×10^7 CTLs. A, Tumor-infiltrating cells were harvested 3 days after CTL transfer and MDSCs were compared with WT and CCR2$^{-/-}$ mice. (*b*) Tumor growth was measured in mice (five to seven mice per group) bearing 9-d B16 tumors w/o 1×10^7 CTL transfer. Suppression of tumor growth by CTLs is augmented in CCR2$^{-/-}$ mice. (*c*) Tumor-infiltrating cells were harvested on day 3, 5, and 7. Cells were gated on CD45$^+$; the infiltration of CTLs into the tumor was compared between WT and CCR2$^{-/-}$ mice. (*d*) The absolute number of CTLs on days 3, 5 and 7 after ACT in WT and CCR2$^{-/-}$ mice. (*e*) Tumor-infiltrating cells were harvested at the indicated time points and stimulated with 1 μg/ml mgp100 peptide. Cells were gated on CD45$^+$CD8$^+$CD90.1$^+$; Externalization of CD107a on CD8$^+$CD90.1$^+$ CTLs was evaluated. Numbers on the images show the percentage of gated cells (mean ± SD). All experiments shown were performed independently at least three times with similar results.

Suppression of pmel-1 proliferation was also diminished by *N*-acetyl-L-cysteine; it was restored to 39.2 ± 2.1% from 4.1 ± 0.3% at an MDSC:CTL ratio of 3:1. Finally, although Nor-NOHA did not restore pmel-1 proliferation at the MDSC:CTL ratio of 3:1, it was slightly increased from 22.9 ± 3.8% to 55.4 ± 5.2% at a ratio of 0.3:1. These results indicate that NO, ROS and Arginase I are all involved in the immunosuppressive activity of MDSCs after ACT.

Both tumor growth suppression and stimulation of monocytic MDSCs by adoptively transferred CTLs is mediated by IFN-γ

To determine the factors responsible for the activation of MDSCs, anti-IFN-γ neutralizing mAb was administered intraperitoneally to ACT mice. On the day of, and 2 days after, CTL transfer, mice received either 500 μg anti-IFN-γ mAb or rat IgG_1 isotype control. Treatment with anti-IFN-γ mAb was found to completely abrogate the anti-tumor activity of transferred CTLs (Fig. 5*a*). Thus, even though mice received CTLs, tumors in anti-IFN-γ mAb-treated mice grew progressively with the same kinetics as in untreated mice. Tumor-infiltrating cells were harvested 3 days after ACT in animals treated or not treated with anti-IFN-γ mAb. The absolute number of tumor infiltrating cells was comparable between these two groups (Fig. 5*b*). The degree of CTL infiltration into the tumor, as well as the level of intra-tumoral IFN-γ expression was the same in anti-IFN-γ mAb-treated and isotype control-treated mice, although slightly but non-significantly reduced in the former (Figs. 5*c* and 5*d*). Nonetheless, the anti-tumor activity of the CTLs was completely abrogated in the anti-IFN-γ mAb-treated mice. The percentage and number of $Gr1^{int}Ly6C^{+}$ monocytic MDSC in the tumor were both decreased by neutralization of IFN-γ although the overall number of tumor infiltrating cells remained the same (Figs. 5*b* and 5*e*). These results indicate that both tumor growth suppression and expansion of monocytic MDSC in the tumor depend on the IFN-γ produced by the tumor-specific CTLs.

The anti-tumor activity of the CTLs is augmented in the absence of monocytic MDSC

To determine the factors responsible for the recruitment of MDSCs into the tumor, mRNA expression of chemokine receptors was compared on $Gr1^{high}Ly6C^{+}$, $Gr1^{int}Ly6C^{+}$ and $Gr1^{low}Ly6C^{-}$ cells after ACT (Fig. 5*f*). While $Gr1^{high}Ly6C^{+}$ granulocytic MDSCs express CCR1, $Gr1^{int}Ly6C^{+}$ monocytic MDSCs expressed CCR2. Consistently, CCR2 ligands, CCL2, CCL7 and CCL12 were expressed in the tumor and up-regulated by ACT (Fig. 5*g*). The up-regulation of CCL7 and CCL12 expression was diminished by anti-IFN-γ treatment. These results suggested that CCR2 axis was involved in the recruitment of monocytic MDSCs into the tumor by ACT.

Therefore, we compared the anti-tumor activity of adoptively-transferred CTLs in $CCR2^{-/-}$ mice. B16 tumor cells were subcutaneously inoculated into C57BL/6 wild-type and $CCR2^{-/-}$ mice. Consistent with our previous report,[20] we found that the $CD11b^{+}Gr1^{int}Ly6C^{+}$ monocytic MDSCs decreased in tumor-infiltrating cells from $CCR2^{-/-}$ mice. However, $CD11b^{+}Gr1^{high}Ly6C^{+}$ granulocytic MDSC were increased from 8.4 ± 1.0% to 21.4 ± 13.4% (Fig. 6*a*). CTLs were then adoptively transferred and tumor-infiltrating cells harvested on day 3. CTLs in the tumor in wild-type mice were accompanied by the accumulation of $CD11b^{+}Gr1^{+}$ cells, especially $Ly6C^{+}$ monocytic MDSC. In contrast, $CD11b^{+}Gr1^{int}Ly6C^{+}$ monocytic MDSC were not present in CTL-treated $CCR2^{-/-}$ mice, which instead accumulated granulocytic MDSC. While 71.5 ± 4.6% of infiltrating cells were monocytic MDSC in wild-type mice, this was only 11.9 ± 2.9% in $CCR2^{-/-}$ mice, which had 62.1 ± 7.4% of granulocytic MDSC (Fig. 6*a*).

As shown in Figure 6*b*, tumors grew progressively not only in wild-type mice, but in $CCR2^{-/-}$ mice as well. As expected, tumor growth was suppressed in mice receiving CTLs by adoptive transfer, and more effectively in the absence of CCR2. These results indicate that the anti-tumor activity of transferred CTLs was augmented in the absence of monocytic MDSC accumulation. To investigate the underlying mechanisms for this, tumor-infiltrating cells were harvested and infiltration of CTLs compared at the indicated time points. The percentages of CTLs in infiltrating cells from wild-type mice at days 3, 5 and 7 were 14.9 ± 4.3%, 20.7 ± 6.1% and 13.9 ± 4.7%, respectively (Fig. 6*c*). In CTL-treated $CCR2^{-/-}$ mice, the infiltration of CTLs into the tumor was increased at days 3, 5 and 7 to 31.4 ± 4.7%, 34.1 ± 7.4% and 29.3 ± 2.8%, respectively. The absolute number of CTLs in the tumor was 3.0 ± 1.4 × 10^6 in $CCR2^{-/-}$ mice compared with 1.7 ± 0.8 × 10^6 in wild-type mice on day 5 after CTL transfer (Fig. 6*d*). More $CD107a^{+}$ CTLs were present in the tumor of $CCR2^{-/-}$ mice receiving CTLs (Fig. 6*e*). These results indicated that more CTLs infiltrated into the tumor and exerted better effector function in the absence of monocytic MDSC recruitment.

Discussion

Established tumors comprise multiple cellular constituents.[21] Complex interactions between the different cell types in the tumor contribute to the immunosuppressive microenvironment. Here, we examine the effect of ACT on this complex regulatory network in the tumor. Adoptively-transferred CTLs that infiltrated into the tumor and exerted anti-tumor activity were associated with a massive recruitment of other leukocytes (Supporting Information Fig. S1), the majority of which was a $CD11b^{+}Gr1^{int}Ly6G^{-}Ly6C^{+}$ monocytic MDSC population (Figs. 1, 2 and Supporting Information Fig. S3). This resulted in increased immunosuppressive activity in the tumor microenvironment and suppressed the CTLs, forming a negative feedback loop.

MDSCs were originally identified in tumor-bearing mice as $CD11b^{+}Gr1^{+}$ cells; they are a heterogeneous cellular population containing macrophages, granulocytes, immature DCs and immature myeloid cells.[22,23] They suppress T-cell responses *in vitro* through direct cell-cell contact or by producing arginase I and iNOS.[24] Antigen-specific CD8 T cell tolerance can be induced by nitration of the TCR-CD8 complex mediated by ROS and peroxynitrite produced by MDSCs.[18] They are divided into two populations: monocytic MDSC and granulocytic MDSC[25] which use different effector molecules and signals to suppress antigen-specific T cell responses. In monocytic MDSCs, IFN-γ signaling through STAT1 results in the production of NO.[26] In contrast, granulocytic MDSCs use ROS for their suppressive function.[18] Consistently, in our study, stronger ROS fluorescence intensity was seen in granulocytic MDSCs than monocytic MDSCs (Fig. 3*b*). In ACT, the recruitment of monocytic MDSCs into the tumor

as a result of CTL tumor infiltration outnumbered granulocytic MDSCs (Fig. 2). Therefore, the immunosuppressive activity of CTL-induced monocytic MDSC accumulation was mediated mainly by iNOS, partly by ROS or arginase I (Fig. 4). Both the absolute number of monocytic MDSCs (Fig. 2*b*) and the per cell expression of iNOS mRNA (Fig. 3*a*) were markedly increased in the tumor by ACT, treatment-induced immunosuppressive microenvironment in the tumor turned tougher than that of steady state condition.

We have reported that the robust induction of IFN-γ mRNA and IFN-γ-producing CTLs can be detected in tumors after ACT.[12] Because IFN-γ is a key effector molecule for CTL anti-tumor activity,[27] we investigated its contribution in our B16-pmel-1 CTL model. CTL-inhibited tumor growth was completely prevented by anti-IFN-γ mAb treatment (Fig. 5). This treatment also prevented the accumulation of monocytic MDSC in the tumor in CTL-treated mice. These results suggested that both suppression of tumor growth and the accumulation of monocytic MDSC at the tumor site were functionally dependent on IFN-γ. This is consistent with the report by Gallina *et al.* that MDSC activity was enhanced by IFN-γ released from activated T cells.[28] Monocytes conditioned by tumors express IL-4Rα and secrete IL-13. These two cytokines amplify the expression of iNOS and arginase, which mediate immunosuppression. Consistently, our study demonstrated that IFN-γ produced by adoptively-transferred antigen-specific CTLs augmented immunosuppressive activities of MDSCs in the quantitative as well as the qualitative sense (Figs. 1–3).

To separate anti-tumor activity of ACT from the pro-tumor immunosuppressive activity of MDSC, we studied events downstream of IFN-γ production, notably which chemokine system was involved in this process. It has been reported that the CCL2/CCR2 pathway mediates recruitment of MDSCs into cancers.[29,30] We had previously reported that the CCL2/CCR2 pathway mediates recruitment of myeloid suppressor cells to cancers by controlling both the mobilization of monocytes from the bone marrow to the blood and their migration to the tumor.[20] Although CX3CR1 and CCR5 are also known to be involved in the regulation of monocyte migration,[31,32] tumor-infiltrating macrophages were not reduced in CX3CR1$^{-/-}$ mice and no significant difference was observed in the efficiency of infiltration into tumors by adoptively transferred CCR5$^{+/-}$ and CCR5$^{-/-}$ bone marrow monocytes.[20] In the present study, we demonstrated that monocytic MDSCs recruited into the tumor after ACT strongly express CCR2 (Fig. 5*f*) and CCR2 ligands were induced in the tumor by ACT (Fig. 5*g*). We also demonstrated that ACT induced more profound anti-tumor effects in B16 tumor-bearing CCR2$^{-/-}$ mice in the absence of monocytic MDSC expansion than in wild-type mice (Fig. 6). These results were consistent with previous report of Lesokhin *et al.* that CCR2^{+} monocytic MDSCs accumulated in the GM-CSF secreting tumor and regulated the efficacy of CD8^{+} T cell therapy.[33] Fridlender *et al.* also reported that CCL2 blockade augments cancer immunotherapy.[34] Consistent with our results, anti-CCL2/CCL12 mAb treatment generated more intratumoral CD8^{+} T cells; however, no changes were observed in CD11b^{+}Ly6G^{+} granulocytic MDSCs or in the CD11b^{+}Ly6C^{+} monocytic MDSCs in their model. It remains to be determined whether and which factors might affect recruitment of MDSC subpopulations after ACT, but clearly CCL2, 7 and 12/CCR2 plays an important role in the accumulation of monocytic MDSC at the tumor site associated with ACT.

Despite the presence of granulocytic MDSC in the tumor after ACT possibly compensating for the reduction of monocytic MDSC in CCR2$^{-/-}$ mice, the anti-tumor activity of the infused CTL was not hampered and tumor growth remained profoundly suppressed. This supports the notion that monocytic MDSC, not granulocytic MDSC, were responsible for the ACT-associated immunosuppression. In line with our results, it has been reported that depletion of immune cells in mice before ACT improved the anti-tumor activity of the treatment.[35,36] Nonmyeloablative lymphodepleting preconditioning by systemic chemotherapy also markedly improved the efficacy of adoptive transfer of tumor infiltrating lymphocytes in melanoma patients.[37,38] The ACT-induced recruitment of MDSCs is presumably prevented under these conditions, because myelopoiesis *per se* was inhibited by preconditioning chemotherapy before ACT.

Recently, Landsberg *et al.* reported that melanoma cells acquired ACT resistance through a mechanism involving IFN-γ-dependent PD-L1 upregulation and TNF-α-dependent reversible loss of melanocytic antigens.[39] These two functionally related CTL-induced adaptive mechanisms together contributed to tumor resistance to ACT. Here, we demonstrated that IFN-γ-dependent secondary accumulation of monocytic MDSCs at the tumor site was also involved in this inhibitory process and further amplified the immunosuppressive network.

In conclusion, dual effects of CTL therapy, suppression of tumor growth and but also stimulation of monocytic MDSCs in the tumor, were both mediated by the IFN-γ produced by the infused tumor-specific CTLs. Considering that ACT triggered counter-regulatory immunosuppressive mechanism *via* recruitment of MDSCs, strategies for regulating this step are desired for optimizing ACT.

Acknowledgements

We thank Dr. Nicholas Restifo (National Cancer Institute) for providing the B16F10 tumor cell line, and Takuma Kono for technical assistance.

References

1. Rosenberg SA, Restifo NP, Yang JC, et al. Adoptive cell transfer: a clinical path to effective cancer immunotherapy. *Nat Rev* 2008;8:299–308.
2. Brenner MK, Heslop HE. Adoptive T cell therapy of cancer. *Curr Opin Immunol* 2010;22:251–7.
3. Morgan RA, Dudley ME, Wunderlich JR, et al. Cancer regression in patients after transfer of genetically engineered lymphocytes. *Science* 2006;314:126–9.
4. Robbins PF, Morgan RA, Feldman SA, et al. Tumor regression in patients with metastatic synovial cell sarcoma and melanoma using genetically engineered lymphocytes reactive with NY-ESO-1. *J Clin Oncol* 2011;29:917–24.
5. Kohn DB, Dotti G, Brentjens R, et al. CARs on track in the clinic. *Mol Ther* 2011;19:432–8.

6. Jena B, Dotti G, Cooper LJ. Redirecting T-cell specificity by introducing a tumor-specific chimeric antigen receptor. *Blood* 2010;116:1035–44.
7. Kalos M, Levine BL, Porter DL, et al. T cells with chimeric antigen receptors have potent antitumor effects and can establish memory in patients with advanced leukemia. *Sci Transl Med* 2011;3: 95ra73.
8. Sadelain M. T-cell engineering for cancer immunotherapy. *Cancer J* 2009;15:451–5.
9. Zou W. Immunosuppressive networks in the tumour environment and their therapeutic relevance. *Nat Rev* 2005;5:263–74.
10. Rabinovich GA, Gabrilovich D, Sotomayor EM. Immunosuppressive strategies that are mediated by tumor cells. *Annu Rev Immunol* 2007;25: 267–96.
11. Overwijk WW, Theoret MR, Finkelstein SE, et al. Tumor regression and autoimmunity after reversal of a functionally tolerant state of self-reactive CD8+ T cells. *J Exp Med* 2003;198:569–80.
12. Noji S, Hosoi A, Takeda K, et al. Targeting spatiotemporal expression of CD137 on tumor-infiltrating cytotoxic T lymphocytes as a novel strategy for agonistic antibody therapy. *J Immunother* 2012;35:460–72.
13. Boring L, Gosling J, Chensue SW, et al. Impaired monocyte migration and reduced type 1 (Th1) cytokine responses in C-C chemokine receptor 2 knockout mice. *J Clin Invest* 1997;100:2552–61.
14. Lutz MB, Kukutsch N, Ogilvie AL, et al. An advanced culture method for generating large quantities of highly pure dendritic cells from mouse bone marrow. *J Immunol Methods* 1999; 223:77–92.
15. Betts MR, Brenchley JM, Price DA, et al. Sensitive and viable identification of antigen-specific CD8+ T cells by a flow cytometric assay for degranulation. *J Immunol Methods* 2003;281: 65–78.
16. Eruslanov E, Kusmartsev S. Identification of ROS using oxidized DCFDA and flow-cytometry. *Methods Mol Biol* 2010;594:57–72.
17. Ueha S, Murai M, Yoneyama H, et al. Intervention of MAdCAM-1 or fractalkine alleviates graft-versus-host reaction associated intestinal injury while preserving graft-versus-tumor effects. *J Leukoc Biol* 2007;81:176–85.
18. Nagaraj S, Gupta K, Pisarev V, et al. Altered recognition of antigen is a mechanism of CD8+ T cell tolerance in cancer. *Nat Med* 2007;13:828–35.
19. Youn JI, Nagaraj S, Collazo M, et al. Subsets of myeloid-derived suppressor cells in tumor-bearing mice. *J Immunol* 2008;181:5791–802.
20. Sawanobori Y, Ueha S, Kurachi M, et al. Chemokine-mediated rapid turnover of myeloid-derived suppressor cells in tumor-bearing mice. *Blood* 2008;111:5457–66.
21. Hanahan D, Weinberg RA. Hallmarks of cancer: the next generation. *Cell* 2011;144:646–74.
22. Peranzoni E, Zilio S, Marigo I, et al. Myeloid-derived suppressor cell heterogeneity and subset definition. *Curr Opin Immunol* 2010;22:238–44.
23. Gabrilovich DI, Ostrand-Rosenberg S, Bronte V. Coordinated regulation of myeloid cells by tumours. *Nat Rev Immunol* 2012;12:253–68.
24. Talmadge JE. Pathways mediating the expansion and immunosuppressive activity of myeloid-derived suppressor cells and their relevance to cancer therapy. *Clin Cancer Res* 2007;13:5243–8.
25. Gabrilovich DI, Nagaraj S. Myeloid-derived suppressor cells as regulators of the immune system. *Nat Rev Immunol* 2009;9:162–74.
26. Movahedi K, Guilliams M, Van den Bossche J, et al. Identification of discrete tumor-induced myeloid-derived suppressor cell subpopulations with distinct T cell-suppressive activity. *Blood* 2008;111:4233–44.
27. Schreiber RD, Old LJ, Smyth MJ. Cancer immunoediting: integrating immunity's roles in cancer suppression and promotion. *Science* 2011;331: 1565–70.
28. Gallina G, Dolcetti L, Serafini P, et al. Tumors induce a subset of inflammatory monocytes with immunosuppressive activity on CD8+ T cells. *J Clin Invest* 2006;116:2777–90.
29. Huang B, Lei Z, Zhao J, et al. CCL2/CCR2 pathway mediates recruitment of myeloid suppressor cells to cancers. *Cancer Lett* 2007;252:86–92.
30. Qian BZ, Li J, Zhang H, et al. CCL2 recruits inflammatory monocytes to facilitate breast-tumour metastasis. *Nature* 2011;475:222–5.
31. Geissmann F, Jung S, Littman DR. Blood monocytes consist of two principal subsets with distinct migratory properties. *Immunity* 2003;19:71–82.
32. Tacke F, Alvarez D, Kaplan TJ, et al. Monocyte subsets differentially employ CCR2, CCR5, and CX3CR1 to accumulate within atherosclerotic plaques. *J Clin Invest* 2007;117:185–94.
33. Lesokhin AM, Hohl TM, Kitano S, et al. Monocytic CCR2(+) myeloid-derived suppressor cells promote immune escape by limiting activated CD8 T-cell infiltration into the tumor microenvironment. *Cancer Res* 2012;72:876–86.
34. Fridlender ZG, Buchlis G, Kapoor V, et al. CCL2 blockade augments cancer immunotherapy. *Cancer Res* 2010;70:109–18.
35. Cheever MA, Greenberg PD, Fefer A. Specificity of adoptive chemoimmunotherapy of established syngeneic tumors. *J Immunol* 1980;125: 711–14.
36. North RJ. Cyclophosphamide-facilitated adoptive immunotherapy of an established tumor depends on elimination of tumor-induced suppressor T cells. *J Exp Med* 1982;155:1063–74.
37. Dudley ME, Wunderlich JR, Robbins PF, et al. Cancer regression and autoimmunity in patients after clonal repopulation with antitumor lymphocytes. *Science* 2002;298:850–4.
38. Dudley ME, Wunderlich JR, Yang JC, et al. Adoptive cell transfer therapy following non-myeloablative but lymphodepleting chemotherapy for the treatment of patients with refractory metastatic melanoma. *J Clin Oncol* 2005;23: 2346–57.
39. Landsberg J, Kohlmeyer J, Renn M, et al. Melanomas resist T-cell therapy through inflammation-induced reversible dedifferentiation. *Nature* 2012;490:412–16.

LETTER

doi:10.1038/nature12331

T_{reg} induction by a rationally selected mixture of Clostridia strains from the human microbiota

Koji Atarashi[1,2,3]*, Takeshi Tanoue[1,2]*, Kenshiro Oshima[4,5]*, Wataru Suda[5], Yuji Nagano[1,2], Hiroyoshi Nishikawa[6], Shinji Fukuda[1,7], Takuro Saito[6], Seiko Narushima[1], Koji Hase[1,3], Sangwan Kim[5], Joëlle V. Fritz[8], Paul Wilmes[8], Satoshi Ueha[9], Kouji Matsushima[9], Hiroshi Ohno[1], Bernat Olle[10], Shimon Sakaguchi[6], Tadatsugu Taniguchi[2], Hidetoshi Morita[4,11], Masahira Hattori[5] & Kenya Honda[1,2,4]

Manipulation of the gut microbiota holds great promise for the treatment of inflammatory and allergic diseases[1,2]. Although numerous probiotic microorganisms have been identified[3], there remains a compelling need to discover organisms that elicit more robust therapeutic responses, are compatible with the host, and can affect a specific arm of the host immune system in a well-controlled, physiological manner. Here we use a rational approach to isolate $CD4^+FOXP3^+$ regulatory T (T_{reg})-cell-inducing bacterial strains from the human indigenous microbiota. Starting with a healthy human faecal sample, a sequence of selection steps was applied to obtain mice colonized with human microbiota enriched in T_{reg}-cell-inducing species. From these mice, we isolated and selected 17 strains of bacteria on the basis of their high potency in enhancing T_{reg} cell abundance and inducing important anti-inflammatory molecules—including interleukin-10 (IL-10) and inducible T-cell co-stimulator (ICOS)—in T_{reg} cells upon inoculation into germ-free mice. Genome sequencing revealed that the 17 strains fall within clusters IV, XIVa and XVIII of Clostridia, which lack prominent toxins and virulence factors. The 17 strains act as a community to provide bacterial antigens and a TGF-β-rich environment to help expansion and differentiation of T_{reg} cells. Oral administration of the combination of 17 strains to adult mice attenuated disease in models of colitis and allergic diarrhoea. Use of the isolated strains may allow for tailored therapeutic manipulation of human immune disorders.

$CD4^+FOXP3^+$ T_{reg} cells are present most abundantly in the intestinal mucosa at steady state, and contribute to intestinal and systemic immune homeostasis[4–7]. In germ-free mice, the frequency of colonic T_{reg} cells and levels of IL-10 expression by T_{reg} cells are markedly reduced[4–7]. We have shown previously that a combination of Clostridia strains isolated from conventionally reared mice potently affect the number and function of $CD4^+FOXP3^+$ T_{reg} cells in mouse colonic lamina propria[4]. In an attempt to enable clinical translation of our previous findings, we aimed to identify T_{reg}-cell-inducing bacterial strains derived from the human microbiota (see Supplementary Fig. 1 for a summary of the procedure).

We obtained a human stool sample from a healthy Japanese volunteer. Because we previously reported that the chloroform-resistant fraction of mouse gut microbiota was enriched in T_{reg}-cell-inducing species[4], the stool sample was either untreated or treated with chloroform and orally inoculated into IQI/Jic germ-free mice. Each group of ex-germ-free (exGF) mice was separately housed for 3–4 weeks in vinyl isolators to avoid further microbial contamination. Although a recent study showed that the human microbiota had no impact on the immune responses in the mouse small intestine[8], we observed a significant increase in the percentage of $FOXP3^+$ T_{reg} cells among $CD4^+$ T cells in the colons of exGF mice inoculated with untreated human faeces compared with germ-free mice (Fig. 1a and Supplementary Fig. 2). Notably, a more pronounced increase was observed in the colons of exGF mice inoculated with chloroform-treated human faeces (Fig. 1a). These findings suggest that the human intestinal microbiota contains T_{reg}-cell-inducing bacteria, and that they are enriched in the chloroform-resistant fraction. We also examined the effects of human faeces inoculation on colonic IL-17- and IFN-γ-expressing $CD4^+$ cells (T_H17 and T_H1 cells). In exGF mice inoculated with untreated or chloroform-treated human faeces, the frequency of T_H1 cells was unchanged compared with germ-free mice (Fig. 1b). By contrast, there

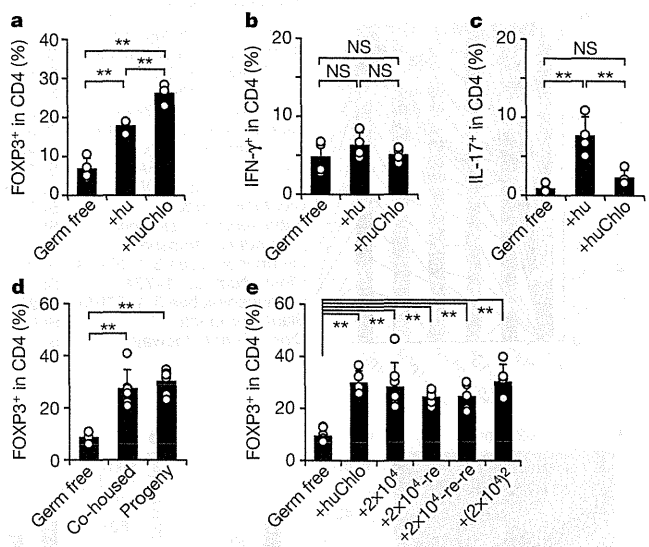

Figure 1 | T_{reg} cell accumulation in germ-free mice induced by inoculation with human microbiota. a–e, The percentages of $FOXP3^+$, $IL\text{-}17^+$ and $IFN\text{-}\gamma^+$ cells within the $CD4^+$ cell population in the colon lamina propria of the indicated mice are shown (see also Supplementary Fig. 2). Circles represent individual animals. The height of the black bars indicates the mean. All experiments were performed more than twice with similar results. Error bars indicate s.d. $^{**}P < 0.01$; NS, not significant. +hu, exGF mice inoculated with untreated human faeces; +huChlo, exGF mice inoculated with chloroform-treated human faeces. (See the main text for further definitions of *x*-axis labels.)

[1]RIKEN Center for Integrative Medical Sciences (IMS-RCAI), 1-7-22 Suehiro-cho, Tsurumi-ku, Yokohama, Kanagawa 230-0045, Japan. [2]Department of Immunology, Graduate School of Medicine, The University of Tokyo, 7-3-1 Hongo, Bunkyo-ku, Tokyo 113-0033, Japan. [3]PRESTO, Japan Science and Technology Agency, 4-1-8 Honcho Kawaguchi, Saitama 332-0012, Japan. [4]CREST, Japan Science and Technology Agency, 4-1-8 Honcho Kawaguchi, Saitama 332-0012, Japan. [5]Graduate School of Frontier Sciences, The University of Tokyo, 5-1-5 Kashiwanoha, Kashiwa, Chiba 277-8561, Japan. [6]Experimental Immunology, Immunology Frontier Research Center, Osaka University, 3-1 Yamadaoka, Suita, Osaka 565-0871, Japan. [7]Institute for Advanced Biosciences, Keio University, 246-2 Mizukami, Tsuruoka, Yamagata 997-0052, Japan. [8]Luxembourg Centre for Systems Biomedicine, University of Luxembourg, Avenue des Hauts-Fourneaux, 7, Esch-sur-Alzette, L-4362, Luxembourg. [9]Department of Molecular Preventive Medicine, Graduate School of Medicine, The University of Tokyo, 7-3-1 Hongo, Bunkyo-ku, Tokyo 113-0033, Japan. [10]PureTech Ventures, 500 Boylston Street, Suite 1600, Boston, Massachusetts 02116, USA. [11]School of Veterinary Medicine, Azabu University, 1-17-71 Fuchinobe, Sagamihara, Kanagawa 252-5201, Japan.
*These authors contributed equally to this work.

was a significant accumulation of T_H17 cells in the colons of exGF mice inoculated with untreated human faeces (Fig. 1c and Supplementary Fig. 2). Notably, the capacity of human faeces to induce T_H17 cells was greatly diminished after treatment with chloroform (Fig. 1c). These results indicate that the chloroform-sensitive bacterial fraction in the human stool tested contained T_H17-cell-inducing bacteria, whereas the chloroform-resistant bacteria preferentially promoted T_{reg} cell accumulation in the colon.

To investigate whether T_{reg} cell induction by the chloroform-resistant fraction of human intestinal bacteria is transmissible, adult germ-free mice were co-housed with exGF mice inoculated with chloroform-treated human faeces for 4 weeks. Co-housed mice showed a significant increase in the frequency of colonic T_{reg} cells (Fig. 1d). In addition, the progeny of exGF mice inoculated with chloroform-treated human faeces also showed increased numbers of T_{reg} cells (Fig. 1d). Therefore, T_{reg} cell induction by human intestinal bacteria is horizontally and vertically transmissible. Oral inoculation of germ-free mice with 2×10^4-fold diluted caecal samples from exGF mice inoculated with chloroform-treated human faeces fully induced the accumulation of T_{reg} cells in the colon lamina propria, suggesting that abundant rather than minor members of the intestinal microbiota in exGF mice inoculated with chloroform-treated human faeces drive the observed induction of T_{reg} cells (Fig. 1e). The T_{reg}-cell-inducing microbiota in mice inoculated with the 2×10^4-fold diluted sample ($+2 \times 10^4$ mice) was a stable community, because serial oral inoculation of caecal contents from these mice equally induced the accumulation of T_{reg} cells in secondary ($+2\times10^4$-re mice) and tertiary recipients ($+2\times10^4$-re-re mice) (Fig. 1e). To minimize nonessential components of the microbiota for T_{reg} cell induction, the caecal contents of $+2 \times 10^4$ mice were again diluted 2×10^4-fold and orally inoculated into another set of germ-free mice ($+(2 \times 10^4)^2$ mice). The $+(2 \times 10^4)^2$ mice had a marked accumulation of T_{reg} cells in the colon (Fig. 1e). These results suggested that we succeeded in obtaining mice colonized with a relatively restricted and stable community of bacterial species enriched for T_{reg} cell inducers.

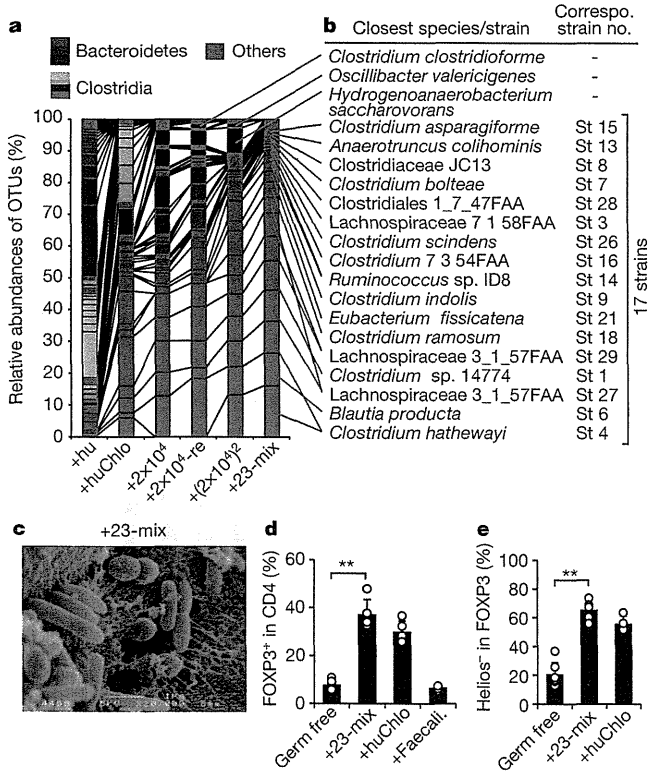

Figure 2 | Assessment of microbiota composition and isolation of T_{reg}-cell-inducing strains. **a**, **b**, Pyrosequencing of 16S rRNA genes was performed on caecal contents from the indicated mice. Relative abundance of OTUs (%) in the caecal bacterial community in each mouse (**a**), and the closest species/strain in the database and the corresponding isolated strain number for the indicated OTU (**b**) are shown. **c**, SEM showing the proximal colon of +23-mix mice. Original magnification, ~×20,000. **d**, **e**, The percentages of $FOXP3^+$ cells within the $CD4^+$ cell population (**d**) and $Helios^-$ cells in $CD4^+FOXP3^+$ cells (**e**) in the colon of the indicated mice. Circles represent individual animals. All experiments were performed more than twice with similar results. Error bars indicate s.d. $^{**}P < 0.01$.

The composition of the gut microbiota in mice treated with human samples was analysed by 16S ribosomal RNA (rRNA) gene amplicon sequencing using a 454 sequencer. Quality filter-passed sequences (3,000 reads for each sample) were classified into operational taxonomic units (OTUs) based on sequence similarity (>96% identity). The numbers of detected reads and closest known species for each OTU are shown in Supplementary Table 1, and the relative abundance of OTUs in each caecal sample is shown in Fig. 2a. As expected, the OTU profiles of mice treated with human faeces were quite different from those of conventional specific pathogen-free (SPF) mice (Supplementary Fig. 3). In mice inoculated with untreated human faeces, OTUs belonging to Bacteroidetes accounted for about 50% of the caecal microbial community (Fig. 2a). By contrast, most OTUs in exGF mice inoculated with chloroform-treated human faeces were related to Clostridia species. Most bacteria in $+2 \times 10^4$, $+2 \times 10^4$-re and $+(2 \times 10^4)^2$ mice had 16S rRNA gene sequence similarities with about 20 species of Clostridia, listed in Fig. 2b.

To isolate bacterial strains with T_{reg}-cell-inducing capabilities, we cultured caecal contents from $+2 \times 10^4$, $+2 \times 10^4$-re and $+(2 \times 10^4)^2$ mice *in vitro* and picked 442 colonies. BLAST searches of 16S rRNA gene sequences of the isolated colonies revealed that 31 strains in total were present, all of which were Clostridia (Supplementary Fig. 4). Of the 31 strains, we selected 23 that had less than 99% 16S rRNA gene sequence identity to any of the other 30 strains (Supplementary Fig. 4). We then individually cultured the 23 strains, mixed them in equal amounts, and orally inoculated the mixture into germ-free IQI mice (+23-mix mice). Numerous rod- and round-shaped bacteria were observed by scanning electron microscopy (SEM) on the epithelial cell surface in +23-mix mice (Fig. 2c), and the size and appearance of the caeca were quite different from those in germ-free mice, indicating successful colonization (Supplementary Fig. 5a). Pyrosequencing of 16S rRNA genes revealed that the caecal microbiota composition in +23-mix mice was quite similar to that in $+(2 \times 10^4)^2$ mice (Fig. 2a). In +23-mix mice, we observed efficient induction of T_{reg} cells in the colonic lamina propria (Fig. 2d). The magnitude was comparable to that observed in exGF mice inoculated with chloroform-treated human faeces and much higher than that in mice colonized with *Faecalibacterium prausnitzii*, a human Clostridia strain well known for enhancing regulatory cell functions[9] (Fig. 2d). Most T_{reg} cells in +23-mix mice expressed low levels of Helios (also known as IKZF2), indicating antigen-experienced cells (Fig. 2e, Supplementary Fig. 5b and ref. 10).

Only 17 strains listed in Fig. 2b and Supplementary Fig. 4 were detected in +23-mix mice by 16S rRNA gene sequencing, indicating that these 17 strains may be sufficient to induce T_{reg} cells. Indeed, we found that the mixture of 17 strains (17-mix) induced $FOXP3^+$ T_{reg} cells to a similar extent as the 23-mix (Fig. 3a). The increase in T_{reg} cells induced by the 17-mix was reproducibly observed in exGF mice of different genetic backgrounds (IQI, BALB/c and C57BL/6) (Fig. 3a). Moreover, the mix was effective in other rodents: the frequency of colonic T_{reg} cells in exGF rats inoculated with 17-mix was significantly higher than that in germ-free rats and comparable to that in SPF rats (Fig. 3a). The colonization with 17-mix induced a significant increase in the frequency of $IL\text{-}10^+$ and/or $ICOS^+$ cells within the T_{reg} cell population, as revealed by analysis of exGF IL-10 reporter mice (*Il10*^{Venus} mice, ref. 4) colonized with the 17-mix (Fig. 3b). Furthermore, $IL\text{-}10^+$ T_{reg} cells in

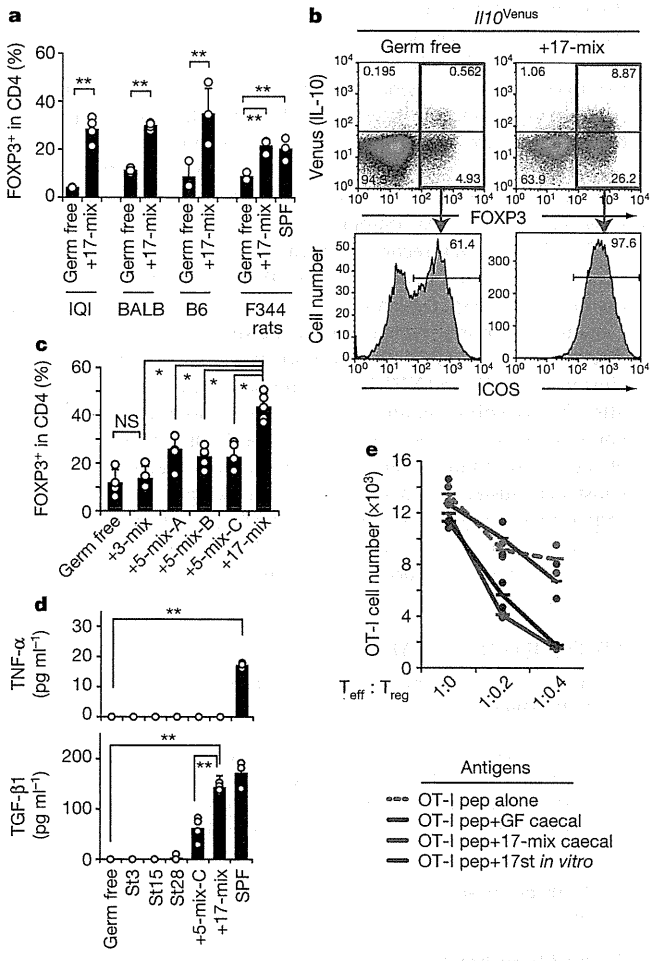

Figure 3 | Characterization of 17 T_{reg}-cell-inducing strains. **a**, The percentages of $FOXP3^+$ cells within the $CD4^+$ cell population in the colon lamina propria of the indicated mice and rats. **b**, The expression of Venus (IL-10) and FOXP3 by the gated colonic lamina propria $CD4^+$ cells, and ICOS expression by $CD4^+FOXP3^+$ cells in exGF *Il10*^{Venus} mice colonized with or without 17-mix. **c**, Percentages of $FOXP3^+$ cells within the $CD4^+$ cell population in IQI exGF mice colonized with the indicated mix. **d**, The production of TNF-α and TGF-β1 in HCT8 cells stimulated with caecal extracts from the indicated mice. **e**, $CD8^+$ T cells from OT-I mice (T_{eff}) and the indicated ratio of colon lamina propria $CD4^+CD25^+$ cells from +17-mix mice (T_{reg}) were incubated with $CD11c^+$ cells pulsed with OT-I peptide alone or in combination with autoclaved caecal contents from +17-mix mice (+17-mix caecal), germ-free mice (+GF caecal), or autoclaved 17 strains cultured *in vitro* (+17 st *in vitro*). Depicted data represent average of duplicates (see also Supplementary Fig. 9c). Circles in **a**, **c**–**e** represent samples from individual animals. All experiments were performed more than twice with similar results. Error bars indicate s.d. $^{**}P < 0.01$; $^{*}P < 0.05$; NS, not significant.

+17-mix mice expressed high levels of CTLA4 (Supplementary Fig. 5c). Because IL-10 and CTLA4 are essential for the immunosuppressive activity of T_{reg} cells[11,12], and ICOS is required for the T_{reg}-cell-mediated suppression of T_H2 responses[13], these results suggest that the mixture of 17 strains affects both the number and function of T_{reg} cells in the colon. Next, we monocolonized germ-free mice with one of each of the 17 individual strains to determine their individual T_{reg} cell induction capability. The monocolonized exGF mice exhibited low to intermediate levels of T_{reg} cell induction with inter-individual variability (Supplementary Fig. 6a). As expected, none of the strains induced T_H17 cells in the monocolonized mice (Supplementary Fig. 6b). We also examined T_{reg} cell induction by subsets of the 17-mix (randomly selected combinations of 3–5 strains: 3-mix, 5-mix-A, 5-mix-B, and 5-mix-C, see Supplementary Fig. 4). Although all tested combinations of 5-mix induced increases in the frequency of T_{reg} cells, the magnitude was substantially lower than that observed in +17-mix mice (Fig. 3c). Therefore, it is likely that the 17 strains act synergistically to amplify the induction of T_{reg} cells in a microbial-community-dependent fashion.

To investigate the mechanism for the T_{reg} cell induction by the community of 17 strains, we incubated various human and mouse intestinal epithelial cell lines and primary cells with aqueous extracts from caecal contents from the +17-mix mice, and assessed the production of the active form of TGF-β1, a key cytokine for the differentiation and expansion of T_{reg} cells. The caecal extracts from +17-mix mice routinely elicited TGF-β1, but not IL-6 and TNF-α, production, and the magnitude was significantly higher than that elicited by caecal extracts from single-strain or 5-mix-colonized mice (Fig. 3d and Supplementary Fig. 7). The induction of TGF-β1 was not inhibited by pre-treatment of the caecal extracts with a protease or nuclease (Supplementary Fig. 7c). Short-chain fatty acids (SCFAs) are protease- and nuclease-insensitive and have been associated with regulation of host immune homeostasis[14]. Quantitative analysis of SCFAs in caecal contents from +17-mix mice showed a significantly higher concentration of acetate, propionate, butyrate and isobutyrate than that in single-strain or 5-mix-colonized mice (Supplementary Fig. 8a). Furthermore, a mixture of sodium salts of these SCFAs elicited TGF-β1 production in epithelial cells to a level similar to that seen when the cells were stimulated with caecal extracts from +17-mix mice (Supplementary Fig. 8b). Therefore, the community of 17 strains cooperatively produces SCFAs that can elicit a TGF-β response, and this activity may contribute to the differentiation and expansion of T_{reg} cells. We also investigated whether the 17 strains provide bacterial antigens to T cells. To do this, we addressed the antigen specificity of T_{reg} cells accumulated in +17-mix mice using a cognate antigen-driven suppression assay. $CD4^+CD25^+$ lamina propria T cells from +17-mix mice substantially inhibited the OT-I ovalbumin (OVA) peptide-driven proliferation of OT-I CD8 T cells, and this suppression was markedly enhanced in the presence of autoclaved caecal content from +17-mix mice or autoclaved 17 strains cultured *in vitro*, but not in the presence of OT-II OVA peptide or caecal content from germ-free mice (Fig. 3e and Supplementary Fig. 9). These results are consistent with previous reports[15,16] and suggest that some fraction of colonic lamina propria T_{reg} cells in +17-mix mice is specific to the 17 strains of Clostridia. Next, we assessed the kinetics of T_{reg} cell accumulation and their expression of Ki67, a cell-cycle-associated nuclear protein, and gut-homing-associated molecules CD103 and β7 integrin. We observed a marked increase in the proportion of Ki67, CD103 and β7 expressing cells by 1 week after inoculation with the 17-mix (Supplementary Figs 10 and 11). Collectively, these observations indicate that the 17 strains provide SCFAs, bacterial antigens and probably other factors, which together contribute to differentiation, expansion and colonic homing of T_{reg} cells.

To define the identity of the 17 bacterial strains fully, we sequenced their genomes (Supplementary Fig. 12). Phylogenetic comparison of the 17 strains using ribosomal multi locus sequencing typing (rMLST) revealed that the 17 strains belong to bacterial species falling within clusters XIVa, IV and XVIII of Clostridia as defined previously[17] (in a recent taxonomy, members of cluster XVIII Clostridia were reclassified in the class Erysipelotrichi) (Supplementary Fig. 13). The genome sequencing also revealed that the 17 strains all lack strong virulence-related genes such as collagenase and phospholipase C, often identified in pathogenic Clostridia species (Supplementary Table 2). We then examined the relative abundance of the 17 strains in healthy and ulcerative colitis human subjects using draft genome sequences of the 17 strains and publicly available human microbiome genomes generated through the MetaHIT project[18]. Ulcerative colitis subjects showed a tendency towards a reduction of the 17 strains, and 5 out of the 17 strains were significantly reduced in ulcerative colitis patients (Supplementary Fig. 14).

To evaluate the potential benefits of supplementation with the 17 strains, 17-mix or control PBS was orally administered into adult SPF

mice every 2 or 3 days (SPF + 17-mix or SPF + ctrl, respectively). We confirmed a significant increase in the frequency of colonic T_{reg} cells in SPF + 17-mix mice compared with SPF + ctrl mice after 3 weeks of treatment (Fig. 4a). While being continuously treated with 17-mix or control, mice were subjected to the OVA-induced allergic diarrhoea model[19]. The occurrence and severity of diarrhoea and the OVA-specific serum IgE levels were significantly reduced in SPF + 17-mix mice relative to control mice (Fig. 4b–d). The protective effect of 17-mix was significantly attenuated by treatment of mice with a T_{reg}-cell-depleting anti-CD25 antibody (Supplementary Fig. 15). We also subjected mice to an experimental colitis model induced by trinitrobenzene sulphonic acid (TNBS)[20]. SPF + 17-mix mice showed less severe colon shortening and milder histological disease features, accompanied by lower mortality than control mice (Fig. 4e–g and Supplementary Fig. 16a). In keeping with this clinical outcome, there was significantly increased expression of *Foxp3* and *Tgfb1* mRNA in SPF + 17-mix mice compared with control mice, as well as a tendency towards a reduction of inflammatory cytokine transcripts (Supplementary Fig. 16b). Identical suppression of colitis by 17-mix was also observed in an adoptive transfer model, in which germ-free SCID mice were orally inoculated with faeces from SPF mice together with or without 17-mix and then transferred with $CD4^+CD45RB^{hi}$ T cells (Supplementary Fig. 17).

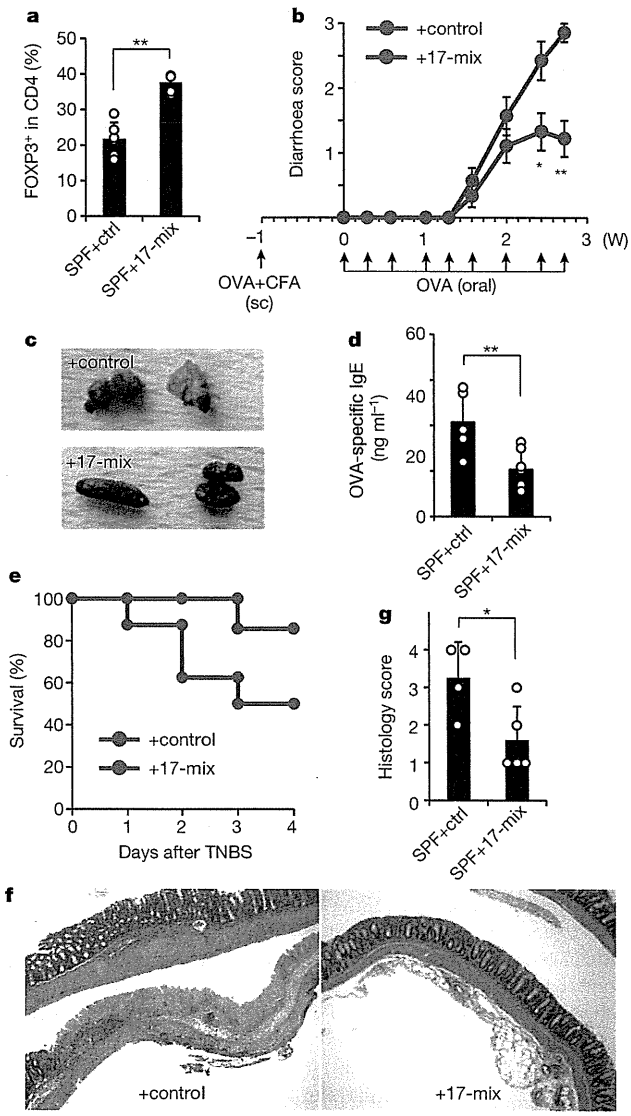

Figure 4 | Treatment with 17-mix suppresses experimental colitis models. **a**, The percentages of $FOXP3^+$ cells within the $CD4^+$ cell population in SPF + 17-mix or SPF + ctrl mice. **b–d**, SPF + 17-mix ($n = 9$) and SPF + ctrl ($n = 7$) mice were subjected to OVA-induced diarrhoea. The diarrhoea score (**b**; see Methods for definition), representative photographs of faeces (**c**), and OVA-specific IgE levels in the sera (**d**) are shown. sc, subcutaneous. **e–g**, SPF + 17-mix ($n = 8$) and SPF + ctrl ($n = 7$) were treated with TNBS. Animal survival (**e**), haematoxylin and eosin staining (original magnification, ×10) (**f**), and histology score of the distal colon (**g**) on day 4 after TNBS administration are shown. Data are representative of two independent experiments. Error bars indicate s.d. $^{**}P < 0.01$; $^{*}P < 0.05$.

The clinical track record of efficacy of single-strain probiotics has been modest. It has been postulated that a collection of functionally distinct bacterial species rationally selected from the human gut microbiota may be more effective than single strains in preventing/treating disease[21]. In the present study, we isolated 17 strains within Clostridia clusters XIVa, IV and XVIII from a human faecal sample; these strains affect T_{reg} cell differentiation, accumulation and function in the mouse colon. It remains to be seen whether the 17 strains will have similar effects in the human intestine; however, a decreased prevalence of Clostridia clusters XIVa and IV in faecal samples from patients with inflammatory bowel disease and atopy[22–24] may suggest that supplementation with the 17-strain bacterial community might counterbalance dysbiosis, induce T_{reg} cells and aid in the management of allergic and inflammatory conditions.

METHODS SUMMARY

Experiments were performed with authorization from the Institutional Review Board for Human Research at RIKEN Yokohama Research Institute. Human stool from a healthy volunteer (Japanese, male, age 31 years) was obtained with informed consent. The sample was mixed with or without chloroform, and the aliquots were inoculated into germ-free IQI mice. Detailed procedures for lamina propria lymphocyte analysis, isolation of bacteria, extraction of bacterial DNA and sequencing are described in Methods. Statistical analysis was performed using the Student's *t*-test.

Full Methods and any associated references are available in the online version of the paper.

Received 14 September 2012; accepted 22 May 2013.
Published online 10 July 2013.

1. Round, J. L. & Mazmanian, S. K. The gut microbiota shapes intestinal immune responses during health and disease. *Nature Rev. Immunol.* **9,** 313–323 (2009).
2. Honda, K. & Littman, D. R. The microbiome in infectious disease and inflammation. *Annu. Rev. Immunol.* **30,** 759–795 (2012).
3. O'Toole, P. W. & Cooney, J. C. Probiotic bacteria influence the composition and function of the intestinal microbiota. *Interdiscip. Perspect. Infect. Dis.* **2008,** 175285 (2008).
4. Atarashi, K. *et al.* Induction of colonic regulatory T cells by indigenous *Clostridium* species. *Science* **331,** 337–341 (2011).
5. Geuking, M. B. *et al.* Intestinal bacterial colonization induces mutualistic regulatory T cell responses. *Immunity* **34,** 794–806 (2011).
6. Russell, S. L. *et al.* Early life antibiotic-driven changes in microbiota enhance susceptibility to allergic asthma. *EMBO Rep.* **13,** 440–447 (2012).
7. Round, J. L. & Mazmanian, S. K. Inducible $Foxp3^+$ regulatory T-cell development by a commensal bacterium of the intestinal microbiota. *Proc. Natl Acad. Sci. USA* **107,** 12204–12209 (2010).
8. Chung, H. *et al.* Gut immune maturation depends on colonization with a host-specific microbiota. *Cell* **149,** 1578–1593 (2012).
9. Sokol, H. *et al. Faecalibacterium prausnitzii* is an anti-inflammatory commensal bacterium identified by gut microbiota analysis of Crohn disease patients. *Proc. Natl Acad. Sci. USA* **105,** 16731–16736 (2008).
10. Thornton, A. M. *et al.* Expression of Helios, an Ikaros transcription factor family member, differentiates thymic-derived from peripherally induced $Foxp3^+$ T regulatory cells. *J. Immunol.* **184,** 3433–3441 (2010).
11. Rubtsov, Y. P. *et al.* Regulatory T cell-derived interleukin-10 limits inflammation at environmental interfaces. *Immunity* **28,** 546–558 (2008).
12. Wing, K. *et al.* CTLA-4 control over $Foxp3^+$ regulatory T cell function. *Science* **322,** 271–275 (2008).
13. Zheng, Y. *et al.* Regulatory T-cell suppressor program co-opts transcription factor IRF4 to control T_H2 responses. *Nature* **458,** 351–356 (2009).
14. Maslowski, K. M. & Mackay, C. R. Diet, gut microbiota and immune responses. *Nature Immunol.* **12,** 5–9 (2011).
15. Lathrop, S. K. *et al.* Peripheral education of the immune system by colonic commensal microbiota. *Nature* **478,** 250–254 (2011).
16. Cebula, A. *et al.* Thymus-derived regulatory T cells contribute to tolerance to commensal microbiota. *Nature* **497,** 258–262 (2013).

17. Collins, M. D. *et al.* The phylogeny of the genus *Clostridium*: proposal of five new genera and eleven new species combinations. *Int. J. Syst. Bacteriol.* **44,** 812–826 (1994).
18. Qin, J. *et al.* A human gut microbial gene catalogue established by metagenomic sequencing. *Nature* **464,** 59–65 (2010).
19. Kweon, M. N., Yamamoto, M., Kajiki, M., Takahashi, I. & Kiyono, H. Systemically derived large intestinal $CD4^+$ Th2 cells play a central role in STAT6-mediated allergic diarrhea. *J. Clin. Invest.* **106,** 199–206 (2000).
20. Strober, W., Fuss, I. J. & Blumberg, R. S. The immunology of mucosal models of inflammation. *Annu. Rev. Immunol.* **20,** 495–549 (2002).
21. Lawley, T. D. *et al.* Targeted restoration of the intestinal microbiota with a simple, defined bacteriotherapy resolves relapsing *Clostridium difficile* disease in mice. *PLoS Pathog.* **8,** e1002995 (2012).
22. Frank, D. N. *et al.* Molecular-phylogenetic characterization of microbial community imbalances in human inflammatory bowel diseases. *Proc. Natl Acad. Sci. USA* **104,** 13780–13785 (2007).
23. Manichanh, C. *et al.* Reduced diversity of faecal microbiota in Crohn's disease revealed by a metagenomic approach. *Gut* **55,** 205–211 (2006).
24. Candela, M. *et al.* Unbalance of intestinal microbiota in atopic children. *BMC Microbiol.* **12,** 95 (2012).

Supplementary Information is available in the online version of the paper.

Acknowledgements This work was supported by JSPS NEXT program, Grant in Aid for Scientific Research on Innovative Areas 'Genome Science' from the Ministry of Education, Culture, Sports, Science and Technology of Japan (No.221S0002), the global COE project of 'Genome Information Big Bang' and the Waksman Foundation of Japan Inc. We thank M. Suyama, K. Furuya, C. Yoshino, H. Inaba, E. Iioka, Y. Takayama, M. Kiuchi, Y. Hattori, N. Fukuda and A. Nakano for technical assistance, and P. D. Burrows for review of the manuscript.

Author Contributions K.Ho. planned experiments, analysed data and wrote the paper together with B.O. and M.H.; K.A. and T.Tano. performed immunological analyses and bacterial cultures together with Y.N., S.N. and H.M.; W.S., K.O., S.K. and M.H. performed bacterial sequence analyses; K.M. and S.U. provided essential materials; H.N., T.S. and S.S. supervised the T_{reg} cell suppression assay; S.F., K.Ha., H.O., T.Tani., J.V.F. and P.W. were involved in data discussions.

Author Information All genome sequence data are deposited in DDBJ BioProject ID PRJDB521-543. Reprints and permissions information is available at www.nature.com/reprints. The authors declare competing financial interests: details are available in the online version of the paper. Readers are welcome to comment on the online version of the paper. Correspondence and requests for materials should be addressed to M.H. (hattori@k.u-tokyo.ac.jp) or K.Ho. (kenya@rcai.riken.jp).

METHODS

Mice and rats. C57BL/6, BALB/c, IQI/Jic and CB.17 SCID mice and F344 rats kept under SPF or germ-free conditions were purchased from Sankyo laboratories, Japan SLC, or CLEA Japan. IQI germ-free mice were used unless otherwise indicated. Germ-free and gnotobiotic mice were bred and maintained in vinyl isolators within the gnotobiotic facility of Sankyo laboratories. Germ-free *Il10*^{Venus} mice were generated as previously described[4]. OT-I and OT-II T-cell receptor transgenic mice were purchased from Taconic Farms. All animal experiments were approved by the Animal Research Committee of RIKEN Yokohama Institute and the University of Tokyo.

Chloroform treatment of human stool and generation of gnotobiotic mice. Human stool from a healthy volunteer (Japanese, male, age 31 years) was obtained with informed consent. Human stool and mouse caecal contents were directly frozen at −80 °C, or suspended in 4 times volume (w/v) of phosphate-buffered saline (PBS) + 20% glycerol solution, snap-frozen in liquid nitrogen and stored at −80 °C until use. The frozen stocks were thawed, suspended in 10 times volume (w/v) of PBS, and passed through a 70 μm cell strainer to eliminate clumps and debris. Then suspensions were mixed with chloroform (final concentration 3%), and incubated in a shaking water bath for 60 min. After evaporation of chloroform by bubbling with N_2 gas for 30 min, the aliquots containing the chloroform-resistant fraction of intestinal bacteria were inoculated into germ-free mice by intra-gastric administration (250 μl; per mouse). To generate a series of gnotobiotic mice inoculated with diluted samples, caecal contents from exGF mice were treated with chloroform, diluted with PBS, and inoculated into germ-free IQI mice. The caecal suspensions diluted 2×10^4-fold correspond to 2.5×10^4 bacterial cells per mouse. Each group of exGF mice was individually caged in the gnotobiotic isolator for 3–4 weeks at Sankyo Lab service.

Isolation of intestinal lamina propria lymphocytes and flow cytometry. The colons were collected and opened longitudinally, washed with PBS to remove all luminal contents and shaken in Hanks' balanced salt solution (HBSS) containing 5 mM EDTA for 20 min at 37 °C. After removing epithelial cells, muscle layers and fat tissue using forceps, the lamina propria layers were cut into small pieces and incubated with RPMI1640 containing 4% fetal bovine serum, 0.5 mg ml^{-1} collagenase D, 0.5 mg ml^{-1} dispase and 40 μg ml^{-1} DNase I (all Roche Diagnostics) for 1 h at 37 °C in a shaking water bath. The digested tissues were washed with HBSS containing 5 mM EDTA, resuspended in 5 ml of 40% Percoll (GE Healthcare) and overlaid on 2.5 ml of 80% Percoll in a 15-ml Falcon tube. Percoll gradient separation was performed by centrifugation at 800*g* for 20 min at 25 °C. The lamina propria lymphocytes were collected from the interface of the Percoll gradient and suspended in ice-cold PBS. For analysis of T_{reg} cells, isolated lymphocytes were labelled with the LIVE/DEAD fixable dead cell stain kit (Invitrogen) to exclude dead cells from the analysis. The cells were washed with staining buffer containing PBS, 2% FBS, 2 mM EDTA and 0.09% NaN_3 and surface staining was performed with PECy7- or Pacific blue-labelled anti-CD4 antibody (RM4-5, BD Biosciences), PE-labelled anti-ICOS antibody (C938.4A, BioLegend), Alexa488-labelled anti-CD103 antibody (2E7, BioLegend), and PerCP/Cy5.5-labelled anti-integrin-β7 antibody (FIB27, BioLegend). Intracellular staining of FOXP3, CTLA4, Helios and Ki67 was performed using the Alexa647-labelled anti-FOXP3 antibody (FJK-16 s, eBioscience), PE-labelled anti-CTLA4 antibody (UC10-4F10-11, BD Biosciences), PE-labelled anti-Helios antibody (22F6, BioLegend), PECy7-labelled anti-Ki67 antibody (B56, BD Biosciences) and FOXP3 staining buffer set (eBioscience). For analysis of T_H1 and T_H17 cells, isolated lymphocytes were stimulated for 4 h with 50 ng ml^{-1} phorbol 12-myristate 13-acetate (PMA, Sigma) and 1 μg ml^{-1} ionomycin (Sigma) in the presence of GolgiStop (BD Biosciences). After incubation for 4 h, cells were washed in PBS, labelled with the LIVE/DEAD fixable dead cell stain kit and surface CD4 was stained with PECy7-labelled anti-CD4 antibody. Cells were washed, fixed in Cytofix/Cytoperm, permeabilized with Perm/Wash buffer (BD Biosciences), and stained with the APC-labelled anti-IL-17 antibody (eBio17B7, eBioscience) and FITC-labelled anti-IFN-γ antibody (XMG1.2, BD Biosciences). The antibody-stained cells were analysed with LSR Fortessa or FACSAriaIII (BD Biosciences), and data were analysed using FlowJo software (Treestar).

Meta 16S rRNA gene sequencing. The caecal contents from exGF mice were suspended in 10 ml of Tris-EDTA containing 10 mM Tris-HCl and 1 mM EDTA (pH 8), and incubated with lysozyme (Sigma, 15 mg ml^{-1}) at 37 °C for 1 h with gentle mixing. A purified achromopeptidase (Wako) was added (final concentration 2,000 unit ml^{-1}) and further incubated at 37 °C for another 30 min. Then, sodium dodecyl sulphate (final concentration 1%) was added to the cell suspension and mixed well. Subsequently, proteinase K (Merck) was added (final concentration 1 mg ml^{-1}) to the suspension and the mixture was incubated at 55 °C for 1 h. High-molecular-mass DNA was isolated and purified by phenol/chloroform extraction, ethanol and finally polyethyleneglycol precipitation[25]. PCR was performed using Ex Taq (TAKARA) and (1) the 454 primer A (5′-CCATCTCA TCCCTGCGTGTCTCCGACTCAG (454 adaptor sequence) + barcode (10 bases) + AGRGTTTGATYMTGGCTCAG-3′ (27Fmod)) and (2) the 454 primer B (5′-CCTATCCCCTGTGTGCCTTGGCAGTCTCAG (454 adaptor sequence) + TGCTGCCTCCCGTAGGAGT-3′ (338R)) to the V1–V2 region of the 16S rRNA gene. Amplicons generated from each sample (~330 bp) were subsequently purified using AMPur XP (Beckman Coulter). The amount of DNA was quantified using Quant-iT Picogreen dsDNA assay kit (Invitrogen) and TBS-380mini fluorometer (Turner Biosystems). Then, the amplified DNA was used as template for 454 GS Junior (Roche) pyrosequencing using GS Junior Titanium emPCR Kit-Lib-L, GS Junior Titanium Sequencing Kit and GS Junior Titanium PicoTiterPlate Kit (all Roche) according to the manufacturer's instructions. Quality-filter-passed reads were obtained by removing reads that did not have both primer sequences, had the average quality value (QV) <25, and were possibly chimaeric[26]. Of the filter-passed reads, 3,000 reads trimming off both primer sequences for each sample were used and subjected to OTU analysis with the cutoff similarity of 96% identity. Representative sequences from each OTU were blasted to Ribosomal Database Project (RDP) of bacterial isolates, our genome database constructed from publically available genome sequences in NCBI and HMP databases, and 16S sequences of the 23 strains obtained in this study.

Isolation of bacterial strains. The frozen stocks of caecal contents from exGF mice were serially diluted with PBS and seeded onto non-selective agar plates (blood liver (BL) agar (Eiken Chemical) or Eggerth-Gagnon (EG) agar plates). EG agar plates contain the following components (quantities expressed per litre): Lab-Lemco Powder (2.8 g, Oxoid); proteose peptone no. 3 (10.0 g, Difco); yeast extract (5.0 g, Difco); Na_2HPO_4 (4.0 g); D(+)-glucose (1.5 g); soluble starch (0.5 g); L-cystine (0.2 g); L-cysteine-HCl-H_2O (0.5 g); Tween 80 (0.5 g); Bacto agar (16.0 g, Difco); and defibrinated horse blood (50 ml). After culture under aerobic conditions or strictly anaerobic conditions (80% N_2, 10% H_2, 10% CO_2) at 37 °C for 2 or 4 days, individual colonies were picked up and cultured for an additional 2 or 4 days at 37 °C in ABCM broth (Eiken Chemical) or EG agar plate. The isolated strains were collected into EG stock medium (10% glycerol) and stored at −80 °C. To identify the isolated strains, 16S rRNA gene sequences were determined. The 16S rRNA gene was amplified by colony-PCR using KOD FX (TOYOBO) and GeneAmp PCR System9700 (Applied Biosystems) using 16S rRNA gene-specific primer pairs: 8F (5′-AGAGTTTGATCMTGGCTCAG-3′) and 519R (5′-ATTACCGCGGCKGCTG-3′) or 1513R (5′-ACGGCTACCTTGTTACGACTT-3′). The amplification program consisted of one cycle at 98 °C for 2 min, followed by 40 cycles at 98 °C for 10 s, 57 °C for 30 s and 68 °C for 1 min 30 s. Each amplified DNA was purified from the reaction mixture using Illustra GFX PCR DNA and gel band purification kit (GE Healthcare). Sequence analysis was performed using BigDye Terminator V3.1 cycle sequencing kit (Applied Biosystems) and Applied Biosystems 3730xl DNA analyser (Applied Biosystems). The resulting sequences were compared with sequences in RDP database and genome database using BLAST to determine close species/strains.

Bacterial culture of isolated strains. The isolated strains of Clostridia and Erysipelotrichi were cultured in EG broth without horse blood under a strictly anaerobic condition (80% N_2, 10% H_2, 10% CO_2) at 37 °C in an anaerobic chamber (Coy Laboratory Products). To prepare the bacterial mixture, bacterial strains were individually grown in EG broth to confluence and mixed at equal amounts of media volume.

Scanning electron microscopy. Scanning electron microscopy was performed by Filgen, Inc., Japan. The proximal colon was removed from +23-mix mice, cut open longitudinally, prefixed with 2% glutaraldehyde in 0.1 M phosphate buffer (pH 7.4) for 24 h at 4 °C, and then postfixed with 2% osmium tetroxide for 1 h at 4 °C. Fixed samples were dehydrated for 5 min each in sequential baths of 50%, 70%, 90% and 100% ethanol, inserted into a critical point dryer until dry and coated with osmium in an OPC-80N osmium plasma coater (Filgen). Scanning electron micrographs were taken by a JEOL JSM-6320F instrument.

Measurement of organic acids. Organic acid concentrations in caecal contents were determined by gas chromatography-mass spectrometry (GC-MS). Caecal contents (10 mg) were disrupted using 3-mm zirconia/silica beads (BioSpec Products) and homogenized in extraction solution containing 100 μl of internal standard (100 μM crotonic acid), 50 μl of HCl and 200 μl of ether. After vigorous shaking using a Shakemaster neo (Bio Medical Science) at 1,500 r.p.m. for 10 min, homogenates were centrifuged at 1,000*g* for 10 min and then the top ether layer was collected and transferred into new glass vials. Aliquots (80 μl) of the ether extracts were mixed with 16 μl of *N*-tert-butyldimethylsilyl-*N*-methyltrifluoroacetamide (MTBSTFA). The vials were sealed tightly by screwing and heated at 80 °C for 20 min in a water bath, and left at room temperature for 48 h for derivatization. The derivatized samples were run through a 6890N Network GC System (Agilent Technologies) equipped with HP-5MS column (0.25 mm × 30 m × 0.25 μm) and 5973 Network Mass Selective Detector (Agilent Technologies). Pure helium (99.9999%) was used as a carrier gas and delivered at a flow rate of 1.2 ml min^{-1}.

The head pressure was set at 10 p.s.i. with split 10:1. The inlet and transfer line temperatures were 250 °C and 260 °C, respectively. The following temperature program was used: 60 °C (3 min), 60–120 °C (5 °C min^{-1}), 120–300 °C (20 °C min^{-1}). One microlitre quantity of each sample was injected with a run time of 30 min. Organic acid concentrations were quantified by comparing their peak areas with the standards.

Genome sequencing and gene prediction. The genome sequences of 17 T_{reg}-cell-inducing strains were determined by the whole-genome shotgun strategy using a 454GS FLX Ti or Ion PGM sequencer. Each 1–5 μg of the genomic DNA was sheared to obtain DNA fragments. Template DNA was prepared according to the supplier's protocol. The generated sequence data were assembled using Newbler v2.8 software to obtain the draft genome sequences. All genome sequence data were deposited in DDBJ BioProject ID: PRJDB521-543. Protein-encoding genes were predicted using MetaGeneAnnotator software[27]. Putative toxins and virulence factors were searched using the BLASTP program and virulence factor databases, VFDB (http://www.mgc.ac.cn/VFs/main.htm) and MvirDB (http://mvirdb.llnl.gov), with the *e*-value cutoff of 1.0×10^{-10}, the identity >30% and the length coverage >60%.

Phylogenetic tree. Sequences concatenated with genes encoding 26 ribosomal proteins (large subunit L10, L11, L14, L16, L17, L19, L20, L23, L24, L29, L31, L32, L35, L7/L12, and small subunit S10, S12, S13, S15, S16, S17, S20, S20, S21, S3, S4, S7, S8) predicted from the genomes of each strain were used to construct a phylogenetic tree. The sequences of other bacterial species used for the tree construction were obtained from the ribosomal multi-locus sequencing typing (MLST) database[28]. The calculation was performed using the MEGA v5.0 package and the neighbour-joining method with a bootstrap of 1,000 replicates.

Cognate antigen-driven T_{reg} cell suppression assay. Preparation of antigens in caecal contents was performed as previously reported[15]. Caecal contents from germ-free mice or +17-mix mice were collected and suspended in PBS (500 mg ml^{-1}); they were then filtered through a 70-μm mesh, and autoclaved at 121 °C for 15 min. To prepare antigens of bacterial components, the 17 strains of Clostridia were cultured *in vitro*, mixed, washed and suspended with 1 ml PBS, and autoclaved at 121 °C for 20 min. $CD11c^+$ cells were isolated by FACSAriaIII from spleens of SPF C57BL/6 mice and pulsed for 1 h with 0.5 μM SIINFEKL OT-I peptide alone or in combination with either of 5 μM ISQAVHAAHAEINEAGR OT-II peptide, autoclaved caecal contents from +17-mix mice or germ-free mice (diluted 1:200), or autoclaved 17 strains of bacteria cultured *in vitro* (diluted 1:200). The antigen-pulsed $CD11c^+$ cells were plated at 5×10^4 per well in 96-well round-bottomed plates. CD8 T cells (T_{eff} cells) were sorted from spleens of SPF OT-I mice by FACSAriaIII and added to the $CD11c^+$ cell-seeded plates at 5×10^4 per well. Then, $CD4^+CD25^+$ T cells (T_{reg} cells) sorted from colonic lamina propria of +17-mix mice or from spleens of SPF OT-II mice were added to the culture at the indicated ratio of T_{reg} to T_{eff} cells. After 3 days, all cells were harvested, stained with anti-CD4 and anti-CD8 antibodies, and analysed by FACSAriaIII to enumerate the number of CD8 OT-I T cells.

Intestinal epithelial cell stimulation with caecal extracts and SCFAs. To prepare caecal extracts, frozen caecal contents from germ-free, +17-mix or SPF mice were thawed and well suspended in 4 volumes of sterile water. After centrifugation (5,000 r.p.m. for 15 min), transparent supernatants were collected, filtered through 0.22 μm filter and used as caecal extracts. In some experiments, caecal extracts were treated with proteinase K (2 mg ml^{-1}, 55 °C for 1 h; Roche) or nuclease that degrades all forms of DNA and RNA (125 unit ml^{-1}, 37 °C for 4 h; Thermo), and subsequently heated at 95 °C for 5 min to inactivate the enzymes. Human intestinal epithelial cell lines (HCT8, HT29, Caco2, T84 and Colo205) and a mouse epithelial cell line (CMT93) were obtained from ATCC and maintained at 37 °C (5% CO2) in RPMI containing 10% heat-inactivated horse serum (Invitrogen). Cells were cultured at 1.5×10^5 cells in 150 μl medium in 48-well plates and stimulated with 4.5 μl caecal extract for 24 h. Human primary intestinal epithelial cells were obtained from Lonza and maintained at 33 °C (5% CO2) in SmGM-2 medium containing 10% FBS (Lonza) for 1–2 weeks (6×10^4 cells in 48-well plates). The medium was changed to 150 μl SmGM-2 containing 1% FBS before stimulation. Caecal extracts (4.5 μl) were added to the culture and incubated for 24 h. Culture supernatants were collected and the level of the active form of TGF-β1 (Promega), TNF-α (R&D) and IL-6 (R&D) was measured by ELISA. To stimulate epithelial cell lines with SCFAs, sodium salts of acetate, butyrate, propionate and isobutyrate were dissolved in PBS. SCFAs were added to the culture individually (final 0.5 mM) or in combination (final 0.5 mM each), and incubated for 24 h.

TNBS colitis. C57BL/6 SPF adult mice were orally inoculated with 17-mix or control PBS every 2 or 3 days for 3 weeks. 2,4,6-Trinitrobenzene sulphonic acid (TNBS)-induced colitis was induced by the intracolonic administration of 2.5 mg of TNBS (Sigma) in 50% ethanol into anaesthetized mice via a thin round-tip needle. The tip of the needle was inserted 4 cm proximal to the anal verge, and mice were held in a vertical position for 30 s after the injection. All the mice were observed daily and were killed on day 4 after TNBS administration. Colons were fixed with 4% paraformaldehyde, sectioned, and stained with haematoxylin and eosin. The degree of inflammation in the distal part of colon was graded from 0 to 4 as follows: 0, normal; 1, ulcer with cell infiltration limited to the mucosa; 2, ulcer with limited cell infiltration in the submucosa; 3, focal ulcer involving all layers of the colon; 4, multiple lesions involving all layers of the colon, or necrotizing ulcer larger than 1 mm in length.

Allergic diarrhoea. BALB/c SPF adult mice were primed by subcutaneous injection with 1 mg of OVA (Fraction V; Sigma) in 100 μl of Complete Freund Adjuvant (CFA, DIFCO). One week after priming, mice were given 50 mg of OVA dissolved in 200 μl of PBS by intra-gastric administration three times per week. 17-mix or control PBS was orally administered to mice every 2 or 3 days for the entire period of the experiments. Diarrhoea was monitored visually 1 h after each oral OVA challenge. Diarrhoea was scored as follows: 0, normal faeces (solid); 1, moist faeces (semi-solid); 2, mild diarrhoea (loose); and 3, severe diarrhoea (watery). Serum was collected from the cheek vein 1 h after the last OVA challenge and OVA-specific IgE levels were measured by ELISA (Chondrex).

Adoptive $CD4^+CD45RB^{hi}$ T-cell transfer model of colitis. Germ-free CB.17 SCID mice were orally inoculated with SPF faeces together with or without 17-mix of Clostridia. One week later, exGF SCID mice received 4×10^5 $CD4^+CD45RB^{hi}$ T cells by intraperitoneal injection. Naive $CD4^+CD45RB^{hi}$ T cells were isolated from spleens of SPF BALB/c mice by FACS sorting. All the mice were observed daily and were killed on day 14 after T-cell transfer.

25. Morita, H. *et al.* An improved isolation method for metagenomic analysis of the microbial flora of the human intestine. *Microbes Environ.* **22,** 214–222 (2007).
26. Kim, S. W. *et al.* Robustness of gut microbiota of healthy adults in response to probiotic intervention revealed by high-throughput pyrosequencing. *DNA Res.* **20,** 241–253 (2013).
27. Noguchi, H., Taniguchi, T. & Itoh, T. MetaGeneAnnotator: detecting species-specific patterns of ribosomal binding site for precise gene prediction in anonymous prokaryotic and phage genomes. *DNA Res.* **15,** 387–396 (2008).
28. Jolley, K. A. *et al.* Ribosomal multilocus sequence typing: universal characterization of bacteria from domain to strain. *Microbiology* **158,** 1005–1015 (2012).

Coordinated Changes in DNA Methylation in Antigen-Specific Memory CD4 T Cells

Shin-ichi Hashimoto,*,†,‡ Katsumi Ogoshi,* Atsushi Sasaki,† Jun Abe,* Wei Qu,† Yoichiro Nakatani,† Budrul Ahsan,§ Kenshiro Oshima,† Francis H. W. Shand,* Akio Ametani,* Yutaka Suzuki,¶ Shuichi Kaneko,‖ Takashi Wada,‡ Masahira Hattori,† Sumio Sugano,¶ Shinichi Morishita,† and Kouji Matsushima*

Memory CD4$^+$ T cells are central regulators of both humoral and cellular immune responses. T cell differentiation results in specific changes in chromatin structure and DNA methylation of cytokine genes. Although the methylation status of a limited number of gene loci in T cells has been examined, the genome-wide DNA methylation status of memory CD4$^+$ T cells remains unexplored. To further elucidate the molecular signature of memory T cells, we conducted methylome and transcriptome analyses of memory CD4$^+$ T cells generated using T cells from TCR-transgenic mice. The resulting genome-wide DNA methylation profile revealed 1144 differentially methylated regions (DMRs) across the murine genome during the process of T cell differentiation, 552 of which were associated with gene loci. Interestingly, the majority of these DMRs were located in introns. These DMRs included genes such as CXCR6, Tbox21, Chsy1, and Cish, which are associated with cytokine production, homing to bone marrow, and immune responses. Methylation changes in memory T cells exposed to specific Ag appeared to regulate enhancer activity rather than promoter activity of immunologically relevant genes. In addition, methylation profiles differed between memory T cell subsets, demonstrating a link between T cell methylation status and T cell differentiation. By comparing DMRs between naive and Ag-specific memory T cells, this study provides new insights into the functional status of memory T cells. ***The Journal of Immunology*****, 2013, 190: 4076–4091.**

CD4$^+$ T cells are central regulators of both humoral and cellular immune responses. Activation of naive CD4$^+$ T cells by Ag induces cell proliferation, resulting in the formation of a large number of effector cells and, subsequently, a limited number of memory cells. Memory CD4$^+$ T cell populations are maintained by cytokine survival signals and homeostatic proliferation, such that they are able to respond rapidly to subsequent exposure to the same Ag (1, 2). Recently, it was reported that the first exposure of a naive T cell to Ag and cytokine signals results in specific changes in the cell's chromatin structure and in DNA methylation of the cell's cytokine genes (3–5).

Chromatin modifications are known to impose epigenetic controls on gene expression without changing DNA sequence (6). These modifications determine the level of cell type–specific gene transcription by modulating the accessibility of genes to transcription factors and the basal transcription apparatus. It is well known that epigenetic regulation is linked to gene repression of oncogenes and development-related genes (6, 7). Genes that are active (open) in a particular tissue or cell type have increased acetylation and methylation of their histones (e.g., H3K4 methylation), whereas genes that are inactive (closed) are characterized by highly condensed chromatin and decreased acetylation and methylation of their histones (e.g., H3K9 and H3K27 methylation). In addition, DNA methyltransferases establish and maintain the pattern of genomic DNA methylation of cytosines in CpG dinucleotides. DNA methylation status is generally considered to correlate inversely with transcriptional activity, with transcriptionally silent genes being highly methylated and transcriptionally active regions being relatively unmethylated (8, 9). DNA methylation is also associated with epigenetic gene regulation during embryogenesis, genomic imprinting, and X-chromosome inactivation (10, 11).

In the immune system, a lack of methylation at the appropriate loci in T and B lymphocytes is associated with transcription and rearrangement of Ig and TCR genes, as well as with cell lineage–specific expression of CD4, CD8, and CD21 (12–15). When naive T cells differentiate to Th1 cells, but not to Th2 cells, DNase hypersensitive sites appear in the IFN-γ gene (16). Furthermore, the IFN-γ gene is methylated to a lesser extent in human and

*Department of Molecular Preventive Medicine, Graduate School of Medicine, The University of Tokyo, Tokyo 113-0033, Japan; †Department of Computational Biology, Graduate School of Frontier Sciences, The University of Tokyo, Chiba 277-8561, Japan; ‡Division of Nephrology, Department of Laboratory Medicine, Kanazawa University, Kanazawa 920-8641, Japan; §Department of Neurology, Graduate School of Medicine, The University of Tokyo, Tokyo 113-0033 Japan; ¶Department of Medical Genome, Graduate School of Frontier Sciences, The University of Tokyo, Chiba 277-8561, Japan; and ‖Department of Disease Control and Homeostasis, Faculty of Medicine, Kanazawa University, Kanazawa 920-8641, Japan

Received for publication August 20, 2012. Accepted for publication February 13, 2013.

This work was supported by a Grant-in-Aid for Scientific Research (C) and Core Research for Evolution Science and Technology of the Japan Science and Technology Agency. S.-i.H. was supported by the "Genome Information Big Bang" Global Center of Excellence project from the Ministry of Education, Culture, Sports, Science, and Technology of Japan.

The sequences presented in this article have been submitted to the National Center for Biotechnology Information Sequence Read Archive (http://www.ncbi.nlm.nih.gov/sra) under accession number SRP007816.

Address correspondence and reprint requests to Dr. Shin-ichi Hashimoto, Department of Molecular Preventive Medicine, Graduate School of Medicine, The University of Tokyo, Tokyo 113-0033, Japan. E-mail address: hashimot@m.u-tokyo.ac.jp

The online version of this article contains supplemental material.

Abbreviations used in this article: BM, bone marrow; CGI, CpG island; DMR, differentially methylated region; GO, Gene Ontology Consortium Database; MSCC, methyl-sensitive cut counting; P/I, PMA/ionomycin; SAGE, serial analysis of gene expression; TAE, Tris–acetate–EDTA; Tg, transgenic; TSS, transcription start site.

murine Th1 and CD8 effector cells than in naive and Th2 cells. In contrast, the IL-4 and IL-5 genes are less methylated in Th2 cells than in Th1 cells. Treatment of T cells in vitro with drugs that inhibit histone deacetylases or DNA methylation increases IL-4 and IFN-γ expression. Moreover, naive T cells from conditional Dnmt1-knockout mice, which lack DNA (cytosine-5-)-methyltransferase 1, express substantially more IFN-γ and IL-4 after Ag activation, an effect that appears to be mediated, at least in part, by demethylation of the *cis*-regulatory element (17). Recently, it was demonstrated that demethylation of the FOXP3 locus is pivotal for differentiation of $CD4^+CD25^+$ regulatory T cells (18) and that the CpG regions of cell type–specific genes (e.g., IL2RA, CTLA4, and CD40LG) in conventional human $CD4^+$ T cells and regulatory T cells are differentially methylated (19). A limiting DNA methylation affects the proliferative potential of Ag-specific $CD8^+$ T cells with moderate effects on their differentiation to effector and memory $CD8^+$ T cells (20). Additionally, methyl-CpG–binding domain protein 2–deficient mice display reduced memory $CD8^+$ T cell differentiation following acute viral infection (21).

These findings indicate that DNA methylation is crucial for memory T cell development and cytokine production. However, in T cells, the DNA methylation status of only a limited number of genes has been examined. The genome-wide DNA methylation status of memory $CD4^+$ T cells derived from Ag-stimulated naive cells remains unexplored. In this study, we investigated the gene-expression profiles and genome-wide DNA methylation status of naive and Ag-specific memory $CD4^+$ murine T lymphocytes.

Materials and Methods

Mice

BALB/c mice were purchased from Clea (Tokyo, Japan). OVA-specific TCR-transgenic (Tg) mice (DO.11.10; OVA-specific TCR Tg × $RAG2^{-/-}$ mice) were maintained under specific pathogen–free conditions.

Reagents

The anti–CD4-Pacific Blue (RM4-5), anti-CD62L mAb (MEL-14), anti–CD25-PE (7D4), PE-conjugated anti-CD4 mAb (GK1.5-PE), anti–CD44-bio (IM7), anti–CD69-bio (H1.2F3), anti–CD127-bio (A7R34), IFN-γ–FITC (XMG1.2), anti–IL-4–Alexa Fluor 647 (11B11), anti–TNF-α–PE/Cy7 (MP6-XT22), anti-mouse TCR DO11.10-PerCP/Cy5.5 (KJ1-26), and streptavidin-allophycocyanin were purchased from BD Pharmingen and eBioscience.

Generation of effector and memory $CD4^+$ T cells

OVA-specific naive $CD4^+$ T cells were isolated from the spleens of DO11.10-Tg mice. To generate effector cells, naive $CD4^+$ T cells were stimulated with 1 μg/ml an OVA peptide (residues 323–339; ISQAVHAAHAEINEAGRD; synthesized by Sigma Genosys, Hokkaido, Japan) plus allophycocyanin for 5 d in vitro (22). Five million of these cells were transferred i.v. into normal syngeneic BALB/c recipient mice. In most experiments, 4 wk after effector cell transfer, $KJ1^+$ cells from the spleens of recipient mice were sorted by FACSVantage (BD Pharmingen) and used as memory $CD4^+$ T cells.

Assays for cytokine production

Naive effector and memory $KJ\text{-}1^+CD4^+$ T cells were restimulated with PMA (20 ng/ml)/ionomycin (1 μg/ml) (P/I) and brefeldin A (10 μg/ml) for 5 h. Cells were then fixed (Cytofix buffer; BD Pharmingen), permeabilized, stained intracellularly with anti–IFN-γ Ab, anti–IL-4 Ab, or anti–TNF-α Ab or its isotype control, and analyzed using a Gallios Flow Cytometer (Beckman Coulter).

Methyl-sensitive cut counting library construction

The integrity of cDNA was confirmed using an Agilent 2100 Bioanalyzer prior to construction of the methyl-sensitive cut counting (MSCC) libraries. The protocol for MSCC library construction was modified slightly from that described previously (23).

Adapters A1 (5′-TTTCCACTACGCCTCCGCTTTCCTCTCTATGGGCAGTCGGTGATCCGAC-3′) and A2 (5′-CGGTCGGATCACCGACTGCCCATAGAGAGGAAAGCGGAGGCGTAGTGG-3′) contain a 5′ MmeI recognition site and a 5′-CG overhang; adapters B1 (5′-CGCCTTGGCCGTACAGCAGAGCTTACCGCAGAGAATGAGGAACCCGGGGCAG-3′) and B2 (5′-TTTCTGCCCCGGGTTCCTCATTCTCTGCGGTAAGCTCTGCTGTACGGCCAAGGCGNN-3′) contain a 3′-NN overhang and barcode (more information in Supplemental Table I), as described in the Applied Biosystems protocol. To construct the MSCC HpaII library, 1 μg genomic DNA isolated from $CD4^+$ T cells was mixed with 8 U HpaII (New England BioLabs) in 1× NEBuffer I in a 50-μl reaction volume and incubated at 37°C for 12 h. Another 8 U HpaII was added, and the mixture was incubated at 37°C for an additional 3 h. DNA was purified by phenol-chloroform extraction and ethanol precipitation and resuspended in 12.5 μl dH_2O. This 12.5-μl DNA solution was mixed with 1.5 μl a mixture containing 5 μM adaptor A1, 5 μM adaptor A2, and 10 U T4 DNA ligase (Invitrogen) before incubation at 16°C for 12 h. DNA was again purified by phenol-chloroform extraction and ethanol precipitation and resuspended in 8 μl dH_2O. This DNA was run on a 10% nondenaturing Tris–acetate–EDTA (TAE) polyacrylamide gel, and the 60–80-bp band was purified. After ethanol precipitation, the DNA pellet was resuspended in 70 μl a reaction mixture containing 14 U MmeI (New England BioLabs), 50 μM S-adenosyl methionine, and 1× NEBuffer 4. This mixture was incubated at 37°C for 12 h, after which DNA was again purified by phenol-chloroform extraction and ethanol precipitation and resuspended in 13 μl dH_2O. This DNA solution was mixed with 1 μl each 5.8 μM adaptor B1 and B2 and 10 U T4 DNA ligase, and the mixture was incubated at 16°C for 12 h. DNA was again purified and resuspended in 20 μl dH_2O. This DNA solution was mixed with 10 U DNA polymerase I (New England BioLabs), 33 μM 2′-deoxynucleoside 5′-triphosphate, and 1× NEBuffer and incubated at 16°C for 30 min. DNA was again purified and resuspended in 8 μl dH_2O. This DNA was run on a 9% nondenaturing TAE polyacrylamide gel, and the 120–140-bp band was purified. The purified DNA was then amplified by PCR using the primers 5′-CCACTACGCCTCCGCTTTCCTCTCTATGGGCAGTCGGTGAT-3′ and 5′-CTGCCCCGGGTTCCTCATTCTCT-3′. The 20-μl mixture for PCR contained 200 nM of each primer, 200 nM 2′-deoxynucleoside 5′-triphosphate, 1× PS buffer, and 1.25 U PrimeSTAR HS DNA polymerase (TaKaRa) and was run at 98°C for 30 s; 10 cycles at 98°C for 5 s, 62°C for 15 s, 72°C for 1 min; and then 72°C for 10 min. The PCR product was run on a 9% nondenaturing TAE polyacrylamide gel, and the 120–130-bp band was purified. The purified libraries were sequenced with the Applied Biosystems SOLiD4 system, following the manufacturer's protocol. The integrity of the cDNA was confirmed using an Agilent 2100 Bioanalyzer prior to construction of the MSCC libraries. A 1-ng sample of size-fractionated cDNA was used for sequencing reactions.

An MspI control library was constructed in the same manner as the HpaII library, with the following exceptions: in the first step, 100 U MspI (New England BioLabs) was used instead of HpaII, and NEBuffer 2 was used instead of NEBuffer 1, and no amplification was performed following gel purification. All HpaII libraries were normalized to 5 million.

SOLiD BioScope software (version 1.3) was used to determine methyl-sensitive restriction enzyme scores and map MSCC sequence reads (20 bp from the MmeI restriction site) to the mouse genome assembly (NCBI37/mm9). A DNA-methylation score was defined as the sum of tag sequence hits (a plus-strand tag and a minus-strand tag) for each restriction enzyme site, in the absence of repetitive sites, and normalized to 10^6 reads by the specific enzyme. To avoid inaccurate identification of methylation sites, differentially methylated regions (DMRs) were defined as those with a change from 0 tags (high-methylation group) to >10 tags (low-methylation group).

Generation and sequencing of the 5′-serial analysis of gene expression library

A newly developed 5′-end mRNA collection method (24) has extended the range of the original 5′-end serial analysis of gene expression (SAGE) technique. This method initially profiles 25-nucleotide 5′-SAGE tags using a novel strategy that incorporates the oligo-capping method. The 5′-SAGE tags are then ligated directly to a linker for sequencing. The purified libraries were sequenced with a Solexa system, according to the manufacturer's protocol (Illumina). The integrity of the cDNA was confirmed using an Agilent 2100 Bioanalyzer prior to construction of 5′-SAGE libraries. A 1-ng sample of size-fractionated cDNA was used for sequencing reactions with the Illumina GA, performed according to the manufacturer's instructions. We assigned unique tags to RefSeq genes (University of California, Santa Cruz, http/hgdownload.cse.ucsc.edu/goldenPath/mm9/database/) when the start position of the tag was within 500 bp upstream of the transcription start site (TSS), based on RefSeq annotation.